remote sensing

MDPI

Article

From Archive to Orthophoto: Georeferencing Slovenia's Aerial Photography (1953–2005)

Luka Škerjanec [1,2,3], Peter Pehani [1], Primož Čas [1], Žiga Kokalj [1,2], Vasja Bric [4], Nina Bončina [4], Boštjan Pucelj [5] and Aleš Marsetič [1,6,*]

[1] Research Centre of the Slovenian Academy of Sciences and Arts (ZRC SAZU), Novi trg 2, 1000 Ljubljana, Slovenia; luka.skerjanec@zrc-sazu.si (L.Š.); peter.pehani@zrc-sazu.si (P.P.); primoz.cas@zrc-sazu.si (P.Č.); ziga.kokalj@zrc-sazu.si (Ž.K.)
[2] Postgraduate School ZRC SAZU, Novi trg 2, 1000 Ljubljana, Slovenia
[3] Department of Archaeology, Faculty of Arts, University of Ljubljana, Zavetiška ulica 5, 1000 Ljubljana, Slovenia
[4] Geodetic Institute of Slovenia, Jamova cesta 2, 1000 Ljubljana, Slovenia; vasja.bric@gis.si (V.B.); nina.boncina@gis.si (N.B.)
[5] Surveying and Mapping Authority of the Republic of Slovenia, Zemljemerska ulica 12, 1000 Ljubljana, Slovenia; bosstjan.pucelj@gov.si
[6] Slovenian Centre of Excellence for Space Sciences and Technologies SPACE-SI, Aškerčeva cesta 12, 1000 Ljubljana, Slovenia
* Correspondence: ales.marsetic@zrc-sazu.si

Highlights

What are the main findings?

- A tailored workflow successfully georeferenced more than 83,000 heterogeneous historical aerial photographs from 1953–2005.
- High accuracies, with mean RMSE values below 3.3 m, can be achieved through the use of SfM and a well-distributed selection of GCPs.

What are the implications of the main findings?

- Large national analogue archives can be efficiently converted into accurate, analysis-ready geospatial datasets using integrated manual, semi-automated, and automated procedures.
- The resulting multi-decadal dataset enables detailed investigation of long-term environmental, land-use, and landscape change at the national scale.

Abstract

Historical aerial photographs (HAPs) provide unique high-resolution records of past landscapes and are an important source for long-term administrative, environmental, archaeological, and spatial research. However, the large-scale transformation of national analogue archives into geometrically consistent geospatial datasets remains challenging because of heterogeneous image quality, incomplete metadata, and varying camera systems. This paper presents the georeferencing of 83,467 analogue aerial photographs covering Slovenia, acquired between 1953 and 2005. The archive was processed within 18 months, combining manual, semi-automatic, and automated procedures with systematic quality control. Preprocessing included image inspection, radiometric enhancement, fiducial mark extraction, frame masking, and preparation of camera calibration information, with the oldest imagery requiring the greatest manual intervention. Aerial triangulation was performed using a Structure from Motion-based workflow in Agisoft Metashape, supplemented by custom Python scripts. The resulting dataset comprises 45 annual orthophoto mosaics with a spatial resolution of 0.5 m. The resulting orthomosaics achieved accuracies (mean RMSE values) ranging from 1.46 to 3.26 m. The project demonstrates that large national archives of heterogeneous HAPs can be transformed into consistent, analysis-ready geospatial datasets. It

Check for updates

Academic Editor: John Trinder

Received: 23 September 2026
Revised: 27 October 2026
Accepted: 3 November 2026
Published: 6 November 2026

Copyright: © 2026 by the authors. Licensee MDPI, Basel, Switzerland. This article is an open access article distributed under the terms and conditions of the Creative Commons Attribution (CC BY) license.

also represents one of the few reported national-scale efforts to systematically georeference an archive of HAPs spanning more than five decades.

Keywords: historical aerial photographs; photogrammetry; orthorectification; aerial triangulation; Structure from Motion; Agisoft Metashape; bundle adjustment

1. Introduction

Historical aerial photographs (HAPs) constitute a unique source of very high-resolution remote sensing data for reconstructing past landscapes. They provide spatially continuous visual records that can support the analysis of long-term landscape change, including urbanisation, deforestation, forest regrowth, agricultural transformation, and other processes that may have unfolded over several decades [1]. Despite this potential, large parts of national and institutional aerial photo archives remain underused, either because they are stored only as analogue material or because their digital versions are not yet geometrically suitable for spatial analysis.

The main reason for this underuse is the limited availability of accurately georeferenced HAPs. Orthorectification transforms aerial photographs into geometrically corrected orthoimages that can be analysed together with other spatial datasets. Although orthorectification is a standard photogrammetric procedure, its application to historical imagery remains challenging. In many archives, camera calibration reports are incomplete or missing, which complicates the estimation of interior and exterior orientation parameters. In addition, reliable ground control points (GCPs) are difficult to identify because many landscape features have changed, disappeared, or been obscured since the time of acquisition.

Recent advances in computer vision and photogrammetry have renewed interest in archival aerial photographs as a source of data for spatial analysis [2]. Once films or contact prints have been scanned, automated and semi automated processing can substantially reduce the time needed to handle large sets of overlapping images. The resulting products can form durable digital archives of analysis ready orthomosaics and related photogrammetric outputs. In this context, automated or semi automated georeferencing is particularly important, because it converts large image repositories from visual archives into spatial datasets suitable for operational use and scientific analysis.

Structure from Motion (SfM) has become relevant for HAP processing because it combines elements of photogrammetry and computer vision to derive camera orientation parameters and 3D structure from overlapping images. SfM based production of orthomosaics from large HAP blocks compensate for incomplete camera metadata by estimating calibration parameters during bundle adjustment. In addition to orthomosaics, these workflows generate dense point clouds and digital surface models (DSMs), which further extend the value of historical image archives for multi-temporal landscape analysis.

This paper presents a large-scale georeferencing project for analogue aerial photographs from the Slovenian Survey and Mapping Authority's (GURS) archive, covering aerial surveys acquired between 1953 and 2005. Countrywide georeferencing of historical aerial imagery is inherently demanding, particularly under operational constraints. In the project, these constraints included an input dataset of approximately 86,000 aerial photographs, a maximum permissible planimetric error of 10.0 m, and a project duration limited to 18 months. To address these requirements, we developed a customized workflow based on SfM, Agisoft Metashape, and custom Python scripts. The workflow produced annual orthomosaics for Slovenia at a spatial resolution of 0.5 m. To the best of our knowledge, the results of this project place Slovenia among the few countries that have georeferenced a substantial portion of their HAP archives.

https://doi.org/10.3390/rs18213822

1.1. Related Work

The growing importance of HAPs is reflected in the rapid increase in scientific publications on archival aerial imagery and its processing [2]. Earlier work mainly focused on scanning, cataloging, and visual interpretation, whereas recent studies increasingly address georeferencing, orthomosaic production, DSM generation, and multi temporal analysis. HAPs are used in fields such as landscape ecology, geomorphology, archaeology, urban studies, land cover reconstruction, and long term environmental monitoring. Their broader value has also been emphasized in archaeology, where historical aerial archives provide information for site discovery, documentation, heritage management, and landscape change analysis [3,4].

Several studies have demonstrated the potential of HAPs for orthophoto production and quantitative spatial analysis. Pinto et al. [5] used the HAPO workflow to orthorectify and mosaic 74 HAPs using a Direct Linear Transform (DLT) model, obtaining image RMSE values below 6 m. Hong and Roosevelt [6] processed a larger dataset of more than 850 HAPs, generating two orthomosaics with spatial resolutions of up to 0.8 m; their combined approach achieved RMSE values predominantly below 5 m for orthomosaics derived from imagery at scales of 1:60,000 and 1:30,000. Automatic algorithms for georeferencing HAPs have also been developed by Craciun and Le Bris [7] and Kim [8], who reported accuracies of approximately 1–2 m RMSE for smaller datasets. Knuth et al. [9] developed an automated historical SfM workflow that generated digital elevation models (DEMs) and orthomosaics without manual GCP selection and demonstrated its application to more than 500 images from glacier and mountain environments.

SfM is now widely used for processing both modern and historical imagery [10–13]. The method extracts image features, matches homologous points across overlapping photographs, and iteratively estimates interior and exterior orientation parameters through bundle adjustment. This makes it suitable for historical imagery when conventional photogrammetric metadata are incomplete. However, historical aerial surveys differ from modern UAV image blocks because they often consist of near nadir photographs with limited across-track overlap, variable image quality, and incomplete calibration information. These properties can reduce network redundancy and increase sensitivity to poor image matches, weak GCP distribution, and camera model instability.

National and regional aerial photo archives are increasingly being scanned and made accessible across Europe [2]. Nevertheless, georeferencing remains a substantial bottleneck. The temporal span of these archives commonly extends from the early or mid 20th century to the beginning of digital aerial acquisition in the 21st century. Because many collections contain hundreds of thousands or millions of photographs, fully manual photogrammetric workflows are not practical. Operational workflows must therefore combine automation, robust quality control, and targeted manual intervention. Archaeological photogrammetry has addressed similar problems through systems such as OrientAL, which aimed to automate relative and absolute orientation of challenging aerial photographs and to reduce the manual GCPs bottleneck [14]. Related work also explored automatic georeferencing by correlating perspectively transformed image patches against pre-existing orthophotos and DSMs [15].

The processing of HAPs is further complicated by the physical and radiometric condition of the source material. Film negatives and contact prints may be degraded, warped, scratched, stained, annotated, or affected by uneven exposure. Scanning can introduce additional geometric and radiometric artefacts if not carefully controlled. The estimation of orientation parameters becomes especially difficult when calibration reports are missing or incomplete. Previous sensitivity analyses have shown that raw scans often require translation, rotation, and cropping before SfM processing, and that near-nadir archive flight

geometries can be less favorable than that of a highly redundant modern digital image network [16]. Similarly, large radiometric and geometric differences between historical images can reduce the reliability of automatic feature extraction and matching [17]. Traditionally, these limitations have been addressed by manually selecting GCPs that link the historical photographs to a contemporary spatial reference. However, the required number of GCPs increases when images are deformed, poorly textured, or acquired in weak geometric configurations. Several studies have therefore investigated strategies to reduce manual GCP requirements while maintaining positional accuracy [18–21]. Recent optimized workflows have also stressed that quality control is essential when historical photogrammetric products are combined with LiDAR or other contemporary elevation data in multi-temporal analysis [22].

1.2. National-Scale Georeferencing of HAP Archives

National-scale georeferencing of HAPs is no longer exceptional, but processing of entire archives at the national scale is, as far as the literature suggests, still incomplete. The strongest documented examples found are Switzerland, France, Sweden, Finland, Czechia, Slovakia, Greece, Spain, and Denmark.

Switzerland provides the best-documented example of highly automated countrywide processing. The swisstopo SWISSIMAGE HIST programme uses national mapping imagery acquired between 1926 and 1998, with approximately 108,000 photographs processed within the wider programme. Heisig and Simmen processed 8507 photographs acquired between 1985 and 1991, covering the entire 41,285 km² territory of Switzerland. Historical photographs were automatically matched against modern SWISSIMAGE orthophotos, filtered and adjusted in photogrammetric blocks. The resulting orthophotos had an absolute positional accuracy of approximately 1 m, while the workflow reduced human working time by at least a factor of five compared with conventional manual GCP collection [21].

The French BD ORTHO Historique, produced by the Institut national de l'information géographique et forestière, currently provides a complete historical layer for 1950–1965. It was constructed from aerial surveys undertaken between 1947 and 1965 and covers metropolitan France and most French overseas territories [23]. Sweden's Historical Orthophotos programme uses a reference year approach: the nationwide "1960" layer combines the most suitable photographs acquired between 1949 and 1970 because no single survey year provides complete national coverage [24]. The National Land Survey of Finland similarly provides orthophotos covering the whole country and includes historical imagery dating from the 1930s onward, although these data constitute an accumulating multi date archive rather than one uniform early national epoch [25].

Czechia processed approximately 21,000 photographs acquired between 1952 and 1957 to cover about 73,000 km^2. Processing was reported for 2003–2005, while the national Historical Orthophotomap of the 1950s was published as a national product in 2010. The released layer is based primarily on imagery from 1952–1954, with photographs from other years used to fill coverage gaps [26].

The Historical Orthophotomap of the Slovak Republic covers the entire country using photographs acquired mainly between 1949 and 1952. Where imagery from the target period was unavailable, the closest available acquisition date was used. The total number of processed photographs has not been published, but the finished 0.5 m orthophotomap has a reported planimetric positional error of 2.71 m [27].

Greece completed a conventional national photogrammetric project between May 2008 and August 2009. Approximately 12,000 photographs from the 1945 and 1960 surveys were organised into prefectural photogrammetric blocks, covering approximately 135,000 km^2, or the entire Greek territory [28].

Spain and Denmark represent slightly qualified national cases. Spain launched PNOA Histórico in 2008 to preserve and process photogrammetric surveys dating from the late 1920s onward. Its principal historical baseline, the 1956–1957 United States Air Force American Series B, covers mainland Spain and the Balearic Islands but not the Canary Islands, Ceuta, or Melilla. Although historical orthophotos are available nationally, the exact number of photographs incorporated into the final orthomosaics has not been published [29]. Denmark's Basic Cover 1954 consisted of approximately 42,700 source photographs and covered 99.6% of the country, with only a few small islands absent [30].

Overall, national historical orthophoto production has been achieved in several countries. Most projects combine scanned analogue imagery, fiducial or camera calibration information, automatic tie-point extraction, ground- or image-based control, bundle adjustment, DEM-based orthorectification, and manual quality control. The Swiss workflow is the clearest example of automation at national scale, whereas Greece illustrates the considerable control point and labour requirements of a more conventional production model. Importantly, national archive size should not be equated with the number of photographs actually georeferenced: several countries hold hundreds of thousands or millions of digitised photographs without having produced a complete national historical orthophoto epoch [2].

2. Study Area

The study area is the entire territory of the Republic of Slovenia. Slovenia is a Central European country and one of the smallest member states of the European Union. Its total area is 20,271 km^2. The landscape is characterised by highly diverse topography, usually divided into four major macro-regions [31]: the high Alps with peaks exceeding 2500 m and the pre-Alpine hills; the rugged Dinaric Alps; the flat Pannonian Plain with its hilly edge; and the Mediterranean hills influenced by the moderating effect of the Adriatic Sea. The country's coastline is 47 km long. The forest cover is approaching two-thirds, ranking Slovenia among the most densely forested countries in the world.

3. Data

The input data consisted of the scanned images of 85,969 HAPs (91.5% were scans from aerial films and 8.5% from contact prints), HAP metadata, data on aerial cameras, i.e., calibration reports for most of the younger part of the collection, and the Digital Terrain Model of Slovenia and its surroundings at 12.5 m resolution (DTM 12.5), produced in 2005 [32].

3.1. Collections of Aerial Photographs of Slovenia

The collection of HAPs covering Slovenia was created between 1953 and 2005. The archive also includes 483 HAPs acquired by the German Air Force (Luftwaffe) in 1943. From 1953 to 1969, the images were acquired by the Military Geographical Institute (VGI) from Belgrade. From 1970 onward, they were acquired by the Geodetic Institute of Slovenia (GZS). These acquisitions are known as Special Aerial Photography of Slovenia (PAS), because they were undertaken to meet the requirements of various users and applications, including base-map production for motorway construction, the construction and maintenance of state roads, forest management, municipal mapping, earthquake damage assessment, river regulation, and the renewal of the land cadastre. Images acquired for special purposes between 1953 and 1974 are referred to as PAS1 (Figures 1 and 2), whereas those acquired between 1975 and 2005 are referred to as PAS2. After 2005, the PAS collection was no longer expanding because there was no longer a national requirement to store

all vertical metric aerial photography data in one location and no organisation assumed responsibility for doing so.

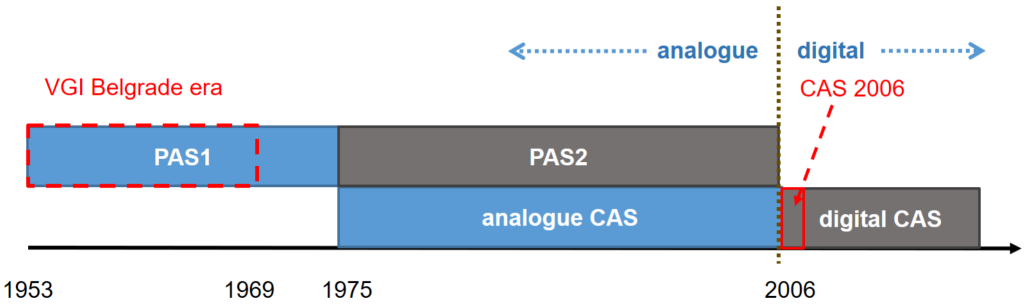


Figure 1. Collections of archival aerial imagery of Slovenia. Upper line: Special Aerial Photography of Slovenia (PAS) collections; lower line: Cyclic Aerial Survey of Slovenia (CAS) collections. In the presented project, only the collections shown in blue were processed, i.e., PAS1 and (analogue) CAS. The red dashed lines mark the years 1953–1969, when the acquisitions were performed by the Military Geographical Institute (VGI) from Belgrade, and the year of the first digital CAS, i.e., 2006.

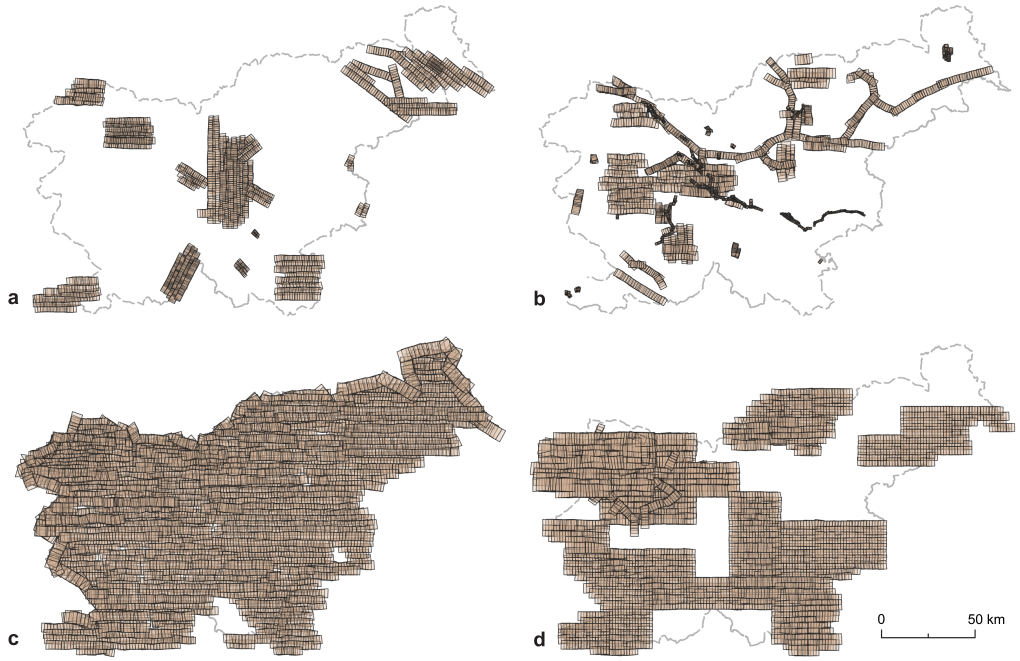


Figure 2. Examples of acquisition coverages from PAS1 1954 (**a**) and 1974 (**b**), and CAS 1975 (**c**) and 2000 (**d**). Coverages from 1954 and 1974 depict the nature of PAS1 acquisitions, which targeted smaller areas or strips scattered across the country. The CAS acquisition from 1975 shows an aim to survey the whole country in a single year (some missing areas were acquired afterwards, in 1976 and 1977). The CAS acquisition from 2000 shows systematic coverage of entire regions, organised in quadrants; combined with CAS coverages from 1998 and 1999, the whole country was covered in a three-year cycle.

In 1975, GZS began the Cyclic Aerial Survey of Slovenia (CAS), primarily to provide systematic data for producing and maintaining national plans and maps (Figures 1 and 2). During the first decade of analogue CAS acquisition (1975–1985), surveys were carried out in a five year cycle. From 1985 to 2005, the cycle was shortened to three years. In 2006, digital aerial cameras were introduced, and the acquisition process already included georeferencing and orthophoto production.

The goal of the project was to process the analogue PAS1 and CAS collections, comprising 85,969 HAPs. During the project only 83,467 HAPs were processed (for details,

see Section 5). Table 1 shows number of HAPs by acquisition year and source type for the processed HAPs. More than 50,000 HAPs from the PAS2 collection are still being scanned.

Systematic metadata collection improved after the establishment of the Slovenian aerial photography service at GZS in 1970. The service used a paper form known as the recording sheet (RS; Slov. snemalni list) to record basic information for each aerial film. The RS includes the RS number, aircraft and camera type, film type and sensitivity, acquisition year, lens and focal length, film cassette, and format. It also records the pilot, navigator, and camera operator, as well as the aerial film number, strip number, aerial photograph number, acquisition date, exposure time, aperture, and filter. A second part of the RS contains data from the photographic laboratory. The quality and completeness of these forms depended on the diligence of the author and varied over time. The RS form underwent several revisions over the years.

For HAPs acquired before 1970 and obtained from the former Yugoslav military archive in Belgrade (VGI), metadata was less complete. Handwritten data on strip envelopes usually included the film number, strip number, work-area name, acquisition year, number of the first and last photograph in the strip, and the number of HAPs in the envelope. Exact acquisition dates were usually not available. Contact prints often lacked additional information, such as strip number and film number.

Table 1. Number of processed HAPs by acquisition year and source type.

PAS1			CAS		
Year	**Contact Prints**	**Film Negatives**	**Year**	**Contact Prints**	**Film Negatives**
1953	41	0	1975	1395	3618
1954	565	1023	1976	0	190
1956	269	1865	1977	0	11
1957	553	85	1980	0	1380
1959	1329	1740	1981	0	1017
1960	94	410	1985	268	3336
1961	6	105	1986	113	2482
1962	9	92	1987	0	2755
1963	237	61	1988	365	3174
1964	264	1507	1989	98	2226
1966	342	411	1990	0	2744
1967	168	736	1991	0	270
1968	70	1741	1992	0	3042
1969	38	1811	1993	0	1550
1970	60	1346	1994	32	2232
1971	160	3584	1995	0	1665
1972	19	2963	1996	0	1454
1973	68	3254	1997	0	2800
1974	117	2796	1998	0	2381
			1999	62	2899
			2000	0	3451
			2001	0	1164
			2002	0	1494
			2003	0	1461
			2004	62	977
			2005	0	1360
Total	4409	25,530	Total	2395	51,133
Total PAS1 + CAS processed: 6804 contact prints; 76,663 film negatives; 83,467 HAPs.					

3.2. Scanning

Analogue HAPs captured on aerial film contain a wealth of spatial information, making high-quality scanning essential for preserving their full information content [33]. In addition to adequate spatial resolution, geometric accuracy also has to be preserved. All available aerial films from the PAS1 and CAS collections were therefore scanned using a Leica DSW700 photogrammetric scanner (Leica Geosystems AG, Heerbrugg, Switzerland). Automation of the scanning process was possible when aerial films were stored on rolls that the scanner could advance and scan sequentially. A special rewinding illumination table was used to inspect aerial films before scanning.

Even though some aerial films were lost, contact prints were generally available for all photographs from all aerial films. However, contact prints contain substantially less detail than the original film negatives. They were scanned using Epson Expression 12000XL (Seiko Epson Corporation, Suwa, Japan), an A3 desktop scanner.

Aerial films were scanned at 2032 DPI, corresponding to 12.5 µm with an 8-bit radiometric resolution. Contact prints were scanned at 1200 DPI, corresponding to 21.2 µm, also at 8-bit. The geometric accuracy of the photogrammetric scanner is better than 2 µm and was checked regularly.

3.3. Database and Metadata

During scanning for each scanned photograph a unique file name was generated from the metadata available to the scanner operator. Usually, the unique name consisted of the year of acquisition, the aerial film number (or strip number if the film number was not known), and the aerial photograph number (copied from the photograph frame).

The scanned archive images were organized in a hierarchical file system. The first folder level represented the acquisition year, the second level represented the film number within that year, and the third level contained the scanned images from the corresponding film. The scanned images were stored as uncompressed TIF rasters.

The metadata for the archive images were organized as a point vector layer in shapefile (SHP) format, with one point per image. The point locations represent approximate initial camera positions at the time of acquisition. These positions were derived by manually transferring the camera positions of the first and last image in each strip from 1:5000 national topographic maps; the positions of intermediate images were then interpolated under the assumption of equidistant spacing. The image metadata include the scanned image name, film number, strip number, acquisition date, suggested maximum use scale, film type, camera manufacturer, lens focal length, regional metadata, and photographer information. Data on the camera model was available through list of camera calibrations.

3.4. Camera Calibration Reports

The calibrations of all analogue large format aerial cameras used between 1970 and 2005 were performed regularly, comprising 18 calibration reports (Table 2).

Table 2. Chronological overview of available camera calibration records from 1970 to 2006, including key information on the aerial cameras and lenses covered by each calibration.

Date of Report	Camera Data			Lens Data		
	Producer	**Model**	**S. No.**	**Model**	**Foc. l. [mm]**	**S. No.**
14-01-1970	Wild	RC5/RC8		15 UAG	152.700	447
28-04-1975	Opton	RMK A 15/23	116195	Pleogon A2	152.980	116255
16-02-1976	Wild	RC5/RC8		15 UAG	152.690	447
14-04-1977	Wild	RC5/RC8		15 UAG II	153.350	3095

Table 2. *Cont*.

Date of Report	Camera Data			Lens Data		
	Producer	**Model**	**S. No.**	**Model**	**Foc. l. [mm]**	**S. No.**
29-03-1978	Zeiss	RMK A 15/23	116195	Pleogon A2	152.964	116254
01-09-1981	Wild	RC5/RC8		15 UAG	152.670	447
10-04-1984	Zeiss	LC 1030	264688/A	Lamegor PL	306.330	7381524A
02-03-1987	Zeiss	LC 1021	267330/A	Lamegoron PL	210.750	7384655A
23-09-1992	Zeiss	LC 1021	267330/A	Lamegoron PL	210.750	7384655A
27-06-1994	Zeiss	RMK A 15/23	116195	Pleogon A2	152.961	116254
16-02-1996	Zeiss	LC 1030	264688/A	Lamegor PL	305.328	7381524A
08-01-1999	Leica	RC30		15/4 UAG-S	153.593	13351
21-01-1999	Zeiss	LC 1021	267330/A	Lamegoron PL	210.745	7384655A
19-02-1999	Zeiss	LC 1021	267330/A	Lamegoron PL	210.749	7384655A
21-01-2002	Leica	RC30		15/4 UAG-S	153.600	13351
03-02-2003	Zeiss	LC 1030	264688/A	Lamegor PL	305.326	7381524A
12-02-2004	Leica	RC30		15/4 UAG-S	153.600	13351
26-01-2006	Leica	RC30		15/4 UAG-S	153.600	13351

For the pre-1970 VGI imagery, only one calibration report was obtained. This report, dated 6 February 1957, is incomplete because it does not include the coordinates of the fiducial marks. High-quality georeferencing of the oldest imagery therefore required additional selection steps (see Section Bundle Adjustment).

3.5. Digital Elevation Models (DEMs)

Most orthorectification procedures used the Digital Terrain Model of Slovenia and its surroundings at 12.5 m resolution (DTM 12.5). This is a homogeneous national DEM compiled from different geodetic sources using weighted aggregation and geomorphological corrections. It is the most recent and reliable national DEM among the classical elevation models, before these were produced from airborne laser scanning (ALS). Compared with newer ALS-derived models, DEM 12.5 is smoother and does not contain bridges or buildings. Its source data is also closer in date to most analogue acquisitions than the dates of more recent ALS-based models. Reported vertical accuracy ranges from 1.1 m in plains to 7.0 m in high mountains.

For the earliest years of PAS1, the time gap between image acquisition and the 2005 DEM exceeds multiple decades. Therefore, initial tests were also performed using an ad hoc DSMs generated from the HAP images themselves through depth map-based 3D reconstruction. The goal was to improve local compatibility between the imagery and the orthorectification surface. This was possible only in areas with adequate image overlap. Consequently, the historical DSMs had to be merged with DTM 12.5 along edge areas without overlap. The results were better in some areas, but the generated surfaces were more locally variable, less homogeneous, and less stable than DTM 12.5. In addition, the seamline between the historical DSM and DTM 12.5 required additional quality control. For these reasons, DTM 12.5 was used for orthorectification.

A modern ALS-derived elevation model from 2011–2015 was used only to assign elevations to GCPs and independent check points (ICPs). Its reported vertical accuracy is 0.15 m.

3.6. Reference Data

The proposed workflow required a reference layer to support the initial matching of HAPs. For this we used two reference datasets. The first was prepared from 9686 colour images acquired during the 2006 CAS campaign, which was the first Slovenian mapping campaign conducted with digital aerial cameras. It was produced in a separate aerotriangu-

lation (AT) process (Figure 3; for details, see Section 4.2) and AT results of CAS 2006 were used directly. This reference data was used to support the initial matching of all HAP blocks from 1992 onwards. For earlier imagery blocks, a processed 1992–1994 CAS block was used as the reference data. This data was itself a product of the HAP processing workflow (for details, see Section Bundle Adjustment).

The required sets of GCPs and ICPs were manually selected from the 2021–2023 national aerial orthophotos, which have a spatial resolution of 0.5 m. According to GURS, the geometric accuracy of these orthophotos is evaluated regionally using independent check points, with no substantial differences observed between regions. The average horizontal accuracy (RMSE) is approximately 0.2 m, while the estimated uncertainty associated with manual point selection is 0.5 pixels (0.25 m).

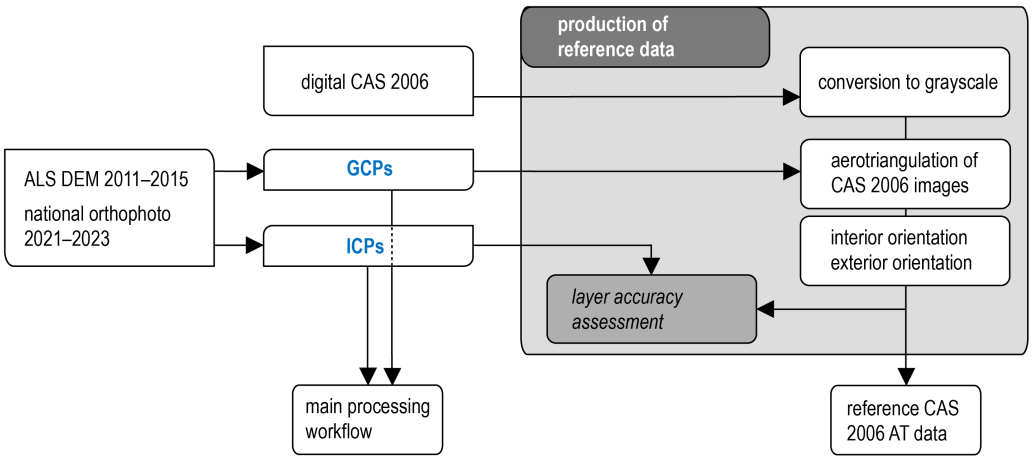


Figure 3. Production of the reference data from CAS 2006 was a separate, one-time process. In the main processing workflow, the results from aerotriangulation (AT) of CAS 2006 images were entered directly; there was no need to produce the 2006 orthomosaic.

4. Methods

The processing workflow for the HAPs consisted of three main stages: (a) preprocessing, including inspection, homogenization, enhancement of available input data, and reconstruction of missing datasets; (b) core photogrammetric processing, consisting of bundle adjustment and orthomosaic generation; and (c) final processing, including the preparation of supplementary products and quality assessment (Figure 4).

The workflow was implemented around Agisoft Metashape Professional (Version 2.1.1 build 17821) [34]. Native Metashape functions were extended through the Python API (2.1.1) [35] using custom scripts for automated project creation, import of external calibration reports, fiducial mark detection and management, GCP and ICP handling, footprint generation, and other processing tasks. Additional Python tools were developed for data preprocessing and supplementary output generation.

4.1. Preprocessing

Preprocessing of the scanned aerial imagery and associated metadata constituted the most time-consuming stage of the workflow. It combined automated and semi automated procedures with manual processing, particularly for imagery from the early PAS1 surveys, where meticulous inspection and correction were required. The preprocessing steps included metadata verification and correction, image orientation and radiometric normalization, frame mask generation, and extraction of fiducial mark locations (Figure 4).

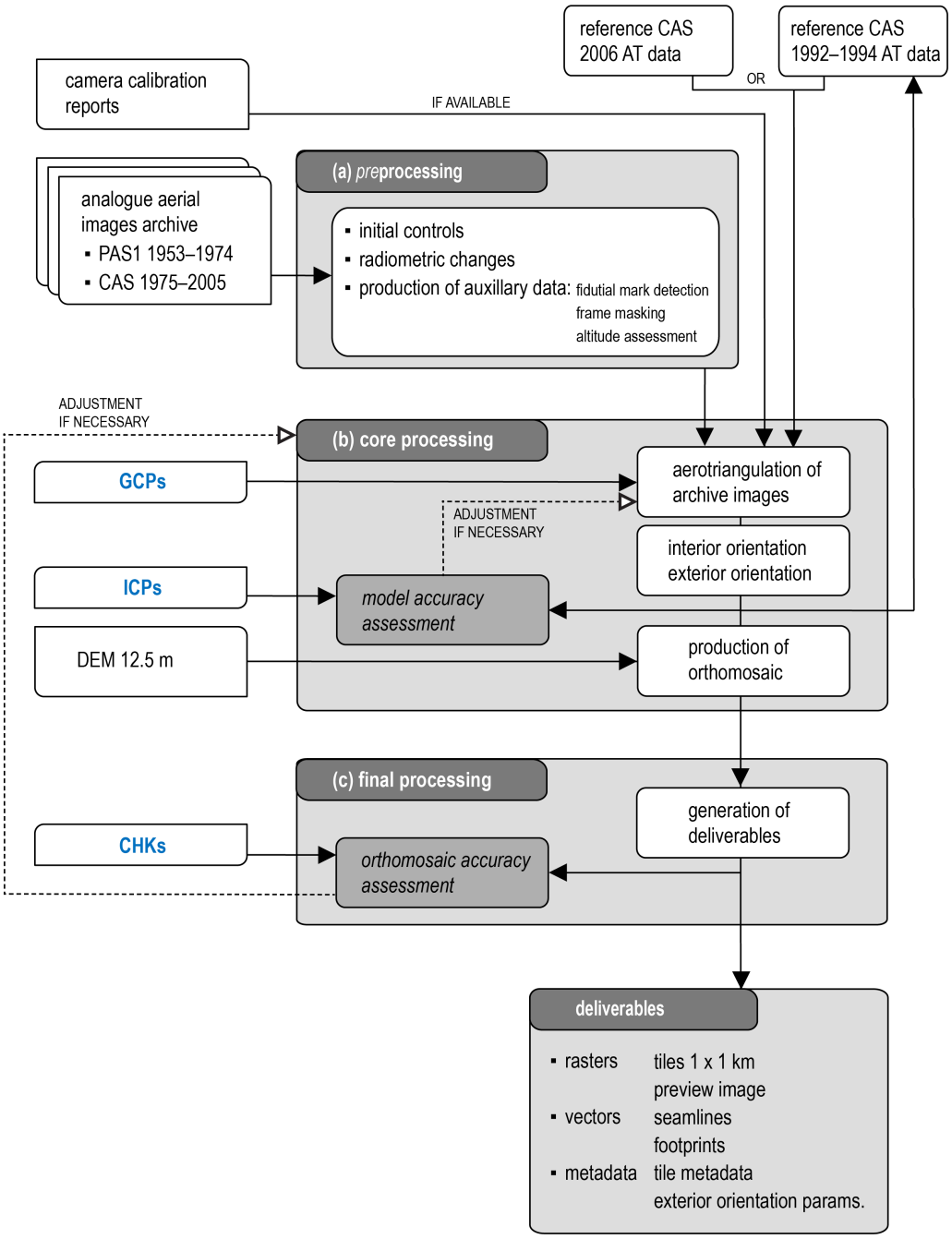


Figure 4. Processing workflow. The main workflow that consisted of three main stages, preprocessing, core processin and final processing, was executed eleven times, for eleven blocks. The deliverables were produced per each year separately.

The first preprocessing stage comprised the verification and standardization of the HAPs and their metadata. These preparatory procedures were critical for ensuring homogeneous input data and the robust execution of subsequent workflow stages (Table 3). In the second preprocessing stage we unifed the radiometric values of all archive images, while in the third stage we produce additional input data (for each image) for the main processing. Task details of the second and third preprocessing stages are described in the following subsections.

Table 3. Tasks of the three preprocessing stages (Figure 4, quadrant (a)).

The first stage: Initial controls
• initial control to detect damaged files that require re-scanning; • generation of JPG thumbnails for all images; • initial visual screening to exclude panoramic or unusable images (e.g., 100% cloud cover, 100% sea) from further processing (for PAS1 images only); • detection and homogenisation of image orientations (for contact print images only); • homogenisation of focal-length metadata (for PAS1 images only); • detection of fiducial-mark type.
The second stage: Radiometric changes
• conversion to grayscale (for three colour films only); • initial image brightening (for identified dark PAS1 contact print images only); • radiometric corrections (for details, see Section 4.1.1).
The third stage: Production of auxillary data
• detection of fiducial marks (for details, see Section 4.1.2); • frame masking (for details, see Section 4.1.3); • estimation of the aircraft altitude at the time of aerial photography (for details, see Section 4.1.4).

4.1.1. Radiometric Corrections

Radiometric preprocessing was performed to improve the consistency of the visual appearance of the HAPs by reducing differences in brightness and contrast. This homogenization was important for producing visually coherent orthophoto mosaics and to help in the image matching stage. The following adjustments were applied.

First, the 179 images acquired on three colour films (1972/25, 1974/55, and 2000/32) were converted to grayscale. Second, contact print images, which were substantially darker than the average image, were brightened using per-image adjusted gamma histogram stretch. Third, radiometric enhancement was applied to all images using Contrast Limited Adaptive Histogram Equalization (CLAHE), as implemented in the OpenCV library (v3.3.1). The CLAHE parameters included a clip limit of 0.7, a tile grid size of 8 × 8, and histogram stretch between the 0.1st and 99.9th percentiles.

Some image-specific artefacts were intentionally not corrected. Vignetting was not addressed because its effect was considered minor relative to radiometric differences between acquisition campaigns and film batches. Similarly, due to time constrains, we did not correct film defects caused by acquisition, development, or long term storage, such as overexposed film edges, stripes at the beginning or end of film rolls, scratches, dust, stains, and repair tape on damaged negatives. We also retained manual annotations, such as areas blacked out to obscure military facilities, grid lines, elevation labels, and infrastructure notes. Image denoising was deliberately omitted to preserve the original radiometric information and fine-scale image detail, and to avoid introducing artifacts or modifying local image textures in ways that could adversely affect feature detection and image matching.

4.1.2. Detection of Fiducial Marks

Over the 52 year acquisition period, the HAPs were captured using cameras manufactured by four companies: Wild, Opton, Zeiss, and Leica. The use of different camera systems resulted in variations in the number, shape, and configuration of fiducial marks (Figure 5).

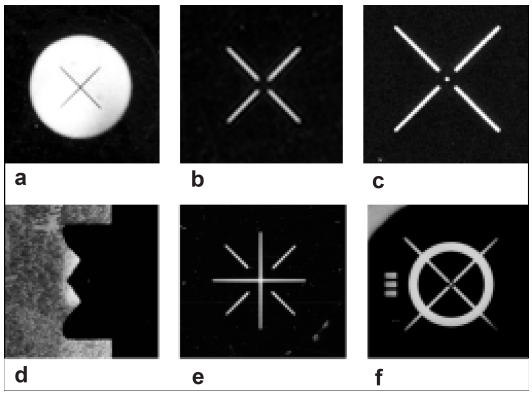


Figure 5. Variations of fiducial mark shapes. Upper row: (**a**–**c**) different generations of fiducial marks in Wild aerial cameras. Lower row: (**d**) fiducial marks of Opton ("pseudo-mark"), (**e**) Zeiss and (**f**) Leica cameras. Wild and Opton images have four fiducial marks. In Wild images, they are located at the four corners, whereas on Opton images, they are centered along the four sides of the image frame. Zeiss and Leica images contain eight marks, four at the corners and four centered along the sides.

Agisoft Metashape includes a generic fiducial mark detection algorithm based on predefined fiducial mark templates for common aerial cameras. This algorithm achieved almost complete detection accuracy for imagery acquired with the Leica RC30 camera, which covers all CAS acquisition campaigns from 1999 onward. Imagery acquired before 1999 with other camera systems, required a combination of automated detection, semi automated quality control, and manual refinement to obtain reliable fiducial mark coordinates.

The main additional procedure was the frame-based fiducial mark detection method available in Metashape. This method requires manual selection of fiducial marks on 10–20 images. Subsequent automatic detections are then based on the average mark positions relative to the image frame.

For Wild and Zeiss images, the standard procedure combined generic automatic detection and frame based detection, followed by two quality control steps. The first control compared the outputs of the two detection methods. The second calculated the mean position of each fiducial mark and the mean distances between fiducial mark pairs for each film number. Marks with large discrepancies in either control step were manually corrected.

Fiducial marks typically include geometric elements such as circles (o), crosses (x, +), or combinations of these forms. In contrast, Opton images contain distinctive pseudo marks consisting of a small white dot inside a black, three-pronged element (Figure 5d). Detection of these pseudo marks was often hindered by small dirt marks near the frame edges. Therefore, an additional procedure was implemented for Opton imagery to search for the brightest small circular object near the provisional fiducial mark location.

Some early PAS1 Wild images contain another fiducial mark type: a black cross inside a white circle (Figure 5a). Detection of these marks on contact print images was difficult because contrast near the image edges was generally weak. We therefore performed a strong local contrast stretch, followed by extraction of the circular form in the frame corner and optimization of the circle centre by image matching against an ideal circle.

4.1.3. Frame Masking

Metashape provides a generic method for automatic masking of dark image frames. This method was used for HAPs after 1998, which were acquired by Leica RC30 and most of which were scanned from film negatives. However, automatic frame masking was not sufficiently reliable for older imagery, especially contact print scans. Consequently, we used a manually guided frame-masking procedure.

For each film, the appropriate mask type was selected based on the "camera type" attribute and confirmed visually. The selected mask was then extensively buffered to avoid edge related anomalies. Finally, the mask was cloned and each clone was resized to match the dimensions of the corresponding image in the film.

4.1.4. Assessment of Camera Positions

Approximate camera position and orientation at the time of acquisition are important input parameters for aero triangulation. Initial camera easting and northing were taken from the corresponding point location available in the metadata.

Aircraft heights were estimated using a simplified formulae [36], in which the scale denominator was multiplied by the focal length. Both values were available in the metadata. The calculation assumed nadir acquisition. In the PAS1 collection, estimated aircraft heights were highly heterogeneous, varying among flight passes from approximately 300 m to 4.5 km above ground. The CAS collection was more homogeneous, mostly spanning from 2 to 6 km.

We set the initial angular orientation parameters for all images to the Metashape defaults, corresponding to nadir acquisition and northward orientation.

4.1.5. Extraction of Ground Control Points, Independent Check Points and Check Points

We used ground control points (GCPs) and independent check points (ICPs) for aero triangulation. To check the quality of the generated orthomosaics, we used separate check points (CHKs) so they could be easily distinguished from ICPs. The extraction of suitable high quality GCPs, ICPs and CHKs proved challenging, as they had to be selected on ground-level or low features that had remained unchanged for more than half a century. As a result, most GCPs, ICPs and CHKs were collected on objects which change very little over time, such as corners of walls around cemeteries or churches, on the bases of narrow objects such as chapels, monuments or electric poles, on park features, on flat object such as airports or crossroads, on linear or rectangular objects such as drywalls, railroad crossings or corners of ruins etc. In mountainous areas, the most suitable features were rocks of various sizes, corners of alpine huts as well as sharp bends in footpaths (Figure 6).

4.2. Preparation of the Reference Data

The reference data was a key component of the workflow. It supported the initial matching of HAPs during the early AT stages and contributed to the generation of a combined tie point cloud.

The reference data was prepared from the first Slovenian digital aerial acquisition, CAS 2006. The 2006 CAS images were accompanied by contemporaneous calibration reports and accurate initial exterior orientation parameters, including camera position (X, Y, Z) and orientation (ϕ, ω, κ). These parameters were derived from campaign metadata, including onboard GPS and INS measurements, and were improved using SIGNAL, the Slovenian network of 16 permanent GNSS stations. The CAS 2006 images underwent an AT procedure that was almost identical to the one later applied to the HAPs (for details, see Section Bundle Adjustment below). The main difference was that CAS 2006 images entered the procedure with accurate exterior orientation parameters, so no external reference data was required.

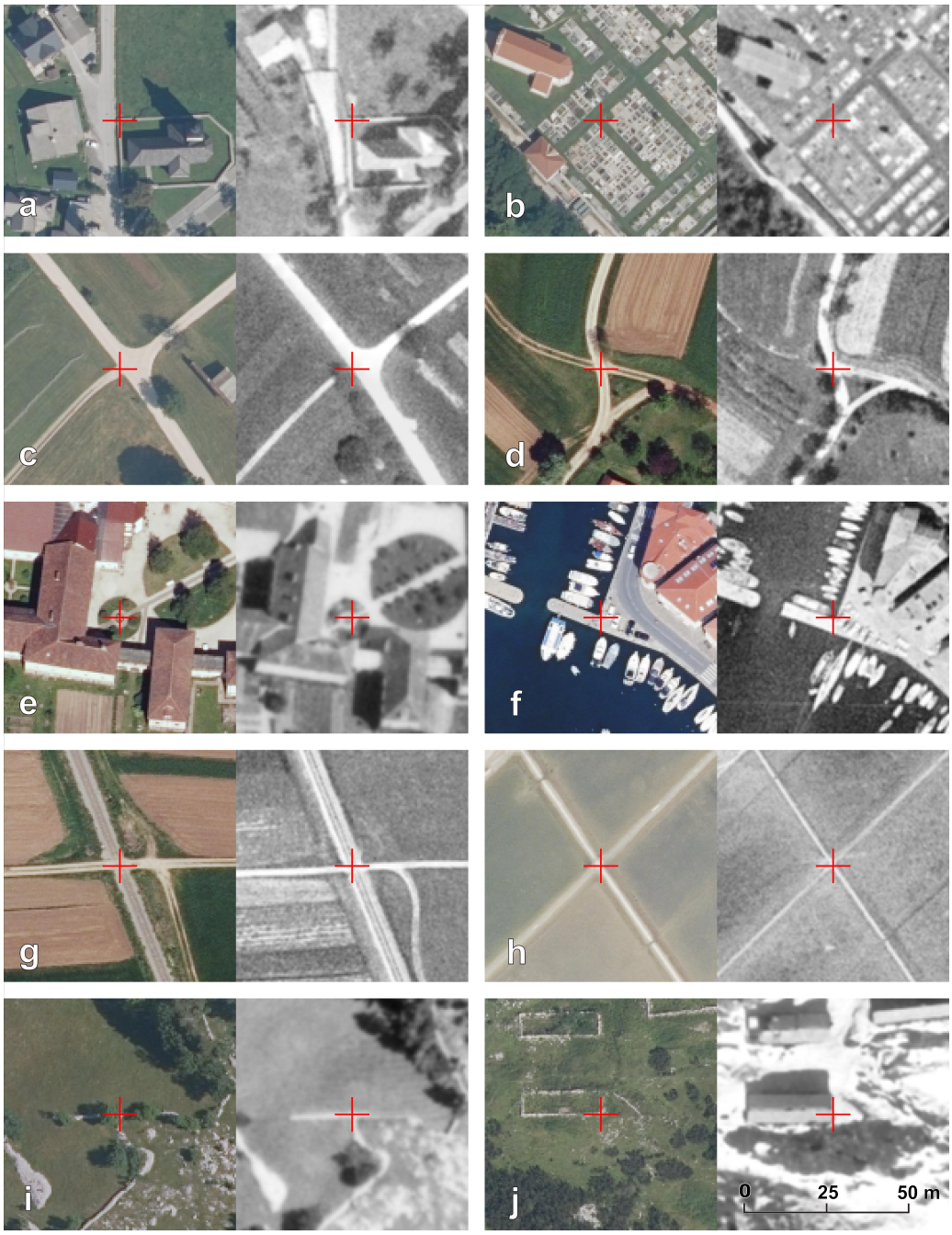


Figure 6. Examples of GCPs, ICPs or CHKs selected on distinct features that have remained stable over several decades. Each image pair shows the 2021–2023 national orthophoto in colour and the 1975 orthomosaic in grayscale. The control points were placed at the (**a**) corner of a cemetery wall, (**b**) a path within a cemetery; (**c**) a four-road junction; (**d**) a three-road junction; (**e**) the center of a courtyard park; (**f**) the edge of a pier; (**g**) a single-track railway crossing; (**h**) a crossroads within a salt-pan grid; (**i**) a dry-stone wall; (**j**) the corner of a First World War mountain barrack. In 1975, the barracks shown in (**j**) were still standing, whereas today they survive only as ruins.

The CAS 2006 images were first converted to grayscale. The images and accompanying reference data (X, Y, Z, ϕ, ω, κ) were imported into Metashape. An initial SfM-based adjustment generated a first sparse tie point cloud and refined camera parameters. Next, 240 GCPs were selected. Their planimetric coordinates were obtained from the current 0.5 m national orthophoto of Slovenia, and their elevations were extracted from current ALS-derived relief data. The GCPs enabled optimization of camera interior and exterior orientation parameters, as well as tie point optimization, through a second SfM-based adjustment. The RMSE

accuracy of the resulting CAS 2006 model, measured at 29 homogeneously distributed ICPs, was 1.03 m.

The CAS 1992–1994 model, which is a product of the processing workflow presented in this article (for details, see Section Bundle Adjustment below), was also used as a reference layer. Its RMSE accuracy, measured at 38 homogeneously distributed ICPs, was 1.40 m (see Table 4 below).

Table 4. Aerial triangulation accuracies given by RMSEs computed at approximately 40 ICPs.

PAS1		CAS	
Years in Block	**ICP RMSE [m]**	**Years in Block**	**ICP RMSE [m]**
1953 *	4.38	1975–1977	1.76
1954 *	4.12, 3.42, 1.61	1980–1981	2.51
1956 *	3.98, 3.14	1985–1987	2.01
1957 *	4.28	1988–1991	1.77
1959 *	3.70, 3.50	1992–1994	1.40
1960 *	3.04	1995–1997	1.85
1961 *	1.31	1998–2000	1.99
1963 *	1.05	2001–2005	1.80
1964 *	2.25, 2.29, 1.24		
1966 *	2.83, 2.83		
1967 *	1.88, 1.48		
1968 *	2.80, 1.90, 2.37		
1969 *	1.77		
1970–1974	3.01		

* The RMSE of aerial triangulation was assessed per partes on individual blocks. The displayed values are for blocks containing at least 100 HAPs (except for 1953, which only contains 32).

4.3. Aerial Triangulation

Aerial triangulation (AT) was the central geometric processing step and provided the basis for generating the CAS 2006 reference data and the annual orthomosaics. AT determines the relative and absolute orientation of overlapping aerial photographs and the 3D coordinates of tie points through bundle adjustment [37]. All AT procedures were performed in Agisoft Metashape using SfM-based feature matching and bundle adjustment. During this process, interior and exterior orientation parameters as well as tie point coordinates were estimated jointly. GCPs and other reference information constrained the image blocks to the target coordinate system.

Bundle Adjustment

The HAPs were processed in several blocks. Each block consisted of 2–8 consecutive years and contained several thousand images (see Table 5). Images were organized into Metashape camera calibration groups with corresponding interior orientation parameters: focal length (f), principal point coordinates (cx, cy), radial lens distortion coefficients (k1, k2, k3), and tangential lens distortion coefficients (p1, p2).

Because reliable estimation of these parameters requires that HAPs from different cameras be handled separately [34], special attention was given to the definition of camera calibration groups. Several grouping rules were tested, including grouping by year, camera type, focal length, scan type, film number, and combinations of these attributes. Empirical testing showed that the best general rule was simultaneous grouping by four attributes: acquisition year, camera type, focal length, and scan type, where scan type distinguished between images from film negatives and images from contact prints. Images with identical values of all four attributes were assigned to the same calibration group.

Table 5. Number of HAPs processed per block of several adjacent years, number of CHKs used to assess accuracy in the block, maximal absolute deviations in both directions (Easting, Northing), and corresponding RMSEs (Easting, Northing, combined) of resulting orthomosaics at 80–156 CHKs per block (note: not all CHKs were used for all blocks).

Years in Block	N. of HAPs	N. of CHKs	Maximal Positional Deviations [m] and RMSEs [m]				
			max|dE|	max|dN|	$RMSE_E$	$RMSE_N$	RMSE
PAS1 1953–1960	7974	80	9.67	6.33	2.52	2.07	3.26
PAS1 1961–1969	7598	156	8.29	7.86	1.61	1.92	2.51
PAS1 1970–1974	14,367	93	6.25	8.29	1.72	1.89	2.55
CAS 1975–1977	5214	98	4.58	6.01	1.50	1.73	2.29
CAS 1980–1981	2397	100	5.00	3.83	1.53	1.45	2.10
CAS 1985–1987	8954	117	5.94	6.25	1.46	1.25	1.92
CAS 1988–1991	8877	112	5.24	5.55	1.31	1.42	1.93
CAS 1992–1994	6856	119	4.13	3.66	1.18	1.02	1.56
CAS 1995–1997	5919	102	4.13	9.01	1.18	1.44	1.86
CAS 1998–2000	8793	120	4.97	2.61	1.31	1.12	1.72
CAS 2001–2005	6518	107	3.30	3.20	1.01	1.05	1.46

In a few cases, this general rule was overridden. If images from a particular film or strip did not align well, they were moved into a separate calibration group. In subsequent optimization steps, the parameters of each group were optimized independently from the parameters of other groups.

Before AT, each HAP was assigned approximate camera coordinates, fiducial marks, and frame masks prepared during preprocessing. Since no initial camera orientation information was available, the rotation angles (ω, ϕ, κ) were initialised to 0° using the default settings in Agisoft Metashape, with an assumed angular accuracy of 10°. This indicated that the angles were only a rough estimate, which is typical for HAPs, which often suffer from film curvature, unknown focal lengths, and aircraft instability. A larger initial tolerance allows the bundle adjustment process to iteratively determine the exact final camera orientation. An a priori positional uncertainty of 50 m was assigned to the camera coordinates, based on the AT results for CAS imagery from 2001–2005, where planimetric discrepancies between the original metadata coordinates and AT-estimated camera positions were below 50 m (see Table 6). The same initial parameters were subsequently applied to all other survey years. During bundle adjustment, these approximate camera positions and orientations were treated as weighted constraints rather than fixed values, allowing substantial adjustments throughout the iterative process. This approach enabled successful AT even for images where discrepancies between the original metadata coordinates and the adjusted camera positions reached several kilometres. For bulk processing, the workflow relied on the capacity of SfM to perform multi-temporal bundle block adjustment and to combine HAPs acquired at different times. In this project, the temporal gap between HAPs and reference imagery reached several decades.

The HAPs were processed in three main steps. First, fiducial marks were used to define the internal coordinate system of each image, either using positions from calibration reports or by internal calibration of fiducial mark geometry using the affine transformation. Second, HAPs were matched to the CAS 2006 reference data through image matching, producing a combined sparse cloud of matched tie points. Because of the very large number of images, matching was performed on downsampled images by a factor of 8 in each dimension. Third, the SfM bundle adjustment step estimated the camera positions and orientations at the time of acquisition and optimized the interior orientation parameters for each calibration group using the Brown–Conrady lens distortion model [38].

Table 6. Annual aerial coverages of orthomosaics (i.e., total area of the produced orthomosaic, coverage of the Slovenia with produced orthomosaic, area of the orthomosaic that extends beyond the country borders) and annual planimetric discrepancies between the original metadata reference positions and the image position estimated using aerotriangulation (i.e., mean, median and RMSE).

Year	N. of Images	Total Area [000 km^2]	Coverage [%]	Out of Slo. [000 km^2]	Mean [m]	Median [m]	RMSE [m]
1953	41	0.171	0.8	0.000	1395.7	1209.3	1631.1
1954	1588	4.632	20.1	0.554	1296.5	742.7	2634.8
1956	2134	4.571	21.9	0.127	932.5	801.7	1104.6
1957	638	5.217	22.7	0.622	1280.3	905.9	1905.9
1959	3069	5.584	24.0	0.724	954.6	720.6	1535.3
1960	504	0.841	4.1	0.000	422.9	362.0	517.9
1961	111	0.240	1.2	0.000	124.9	97.6	160.8
1962	101	0.250	1.2	0.000	306.2	187.2	404.6
1963	298	0.775	3.8	0.001	1092.3	333.9	2832.8
1964	1771	2.471	11.7	0.103	1061.4	447.5	2751.0
1966	753	0.776	3.5	0.066	877.9	552.9	1783.8
1967	904	2.286	11.1	0.035	672.6	473.7	938.6
1968	1811	4.381	20.6	0.198	1.180.8	708.2	2095.6
1969	1849	4.988	23.4	0.236	1519.8	866.4	2978.6
1970	1406	4.061	18.7	0.277	886.4	357.2	2074.5
1971	3744	9.145	40.9	0.851	859.7	702.3	1295.4
1972	2982	5.859	26.5	0.483	921.2	453.3	1997.2
1973	3322	6.857	31.6	0.447	713.8	318.6	1792.9
1974	2913	4.516	21.9	0.066	556.1	204.6	1593.3
1975	5013	22.507	98.0	2.640	640.5	426.8	989.2
1976	190	1.646	7.9	0.053	376.6	293.7	532.0
1977	11	0.083	0.4	0.000	333.7	285.8	372.2
1980	1380	21.175	89.5	3.033	3270.6	678.5	11,307.6
1981	1017	8.756	39.8	0.688	1243.6	491.9	3066.1
1985	3604	9.194	42.1	0.669	614.8	142.1	2710.7
1986	2595	9.068	40.0	0.959	851.8	235.0	3685.3
1987	2755	8.267	36.6	0.840	697.3	646.8	782.5
1988	3539	9.681	44.7	0.617	753.9	635.1	1271.4
1989	2324	7.591	34.0	0.708	620.8	604.5	849.6
1990	2744	8.238	37.0	0.733	264.3	193.0	617.2
1991	270	1.438	6.7	0.071	307.6	266.6	381.4
1992	3042	14.286	66.7	0.770	422.2	268.6	959.7
1993	1550	7.596	34.1	0.681	314.8	211.4	637.5
1994	2264	11.234	51.0	0.892	411.0	257.8	864.8
1995	1665	7.784	34.3	0.830	427.1	291.6	650.0
1996	1454	7.564	33.1	0.863	352.3	260.2	463.0
1997	2800	12.034	52.8	1.338	230.8	139.6	550.9
1998	2381	10.510	44.9	1.401	374.6	201.5	913.0
1999	2961	10.227	43.9	1.325	198.3	47.5	1541.9
2000	3451	15.474	66.2	2.061	57.7	19.4	355.1
2001	1164	5.903	24.3	0.968	36.5	20.4	163.2
2002	1494	6.949	30.3	0.801	19.0	16.7	22.4
2003	1461	6.847	29.1	0.948	19.7	15.6	26.8
2004	1039	5.025	21.6	0.638	20.2	14.8	27.6
2005	1360	6.429	28.6	0.638	10.5	9.4	12.4
Sum/Mean	83,467	302.341	29.9	29.840	652.4	315.5	2157.3

The SfM geometric model combines tie points, GCPs, interior orientation parameters, and exterior orientation parameters (Figure 7). Changes in one set of parameters affect the others, so optimization must be performed iteratively. The optimization followed three consecutive steps. First, additional GCPs were manually selected. Second, the tie point cloud was reduced using accuracy based filtering. Thresholds for reconstruction uncertainty, projection accuracy, and reprojection error were set to 35, 25, and 0.3, respectively, and visible

point cloud outliers were removed. Third, interior and exterior orientation parameters were optimized. These steps were repeated until convergence. Convergence during the iterative AT process was assessed based on the positional errors of GCPs and the estimated camera interior orientation parameters. Convergent behaviour was indicated by decreasing GCP errors between successive iterations, with the objective of achieving positional errors below 10.0 m at all GCPs. In addition, the estimated camera calibration parameters were expected to remain close to their nominal values, with the focal length (f) approaching its specified value and the principal point coordinates (c_x, c_y) remaining near the image centre (0.0, 0.0 mm). Conversely, divergent behaviour was identified by increasing GCP errors and substantial deviations of the estimated calibration parameters from their expected values. In particular, focal length deviations of 2.0 mm or more from the nominal value, and principal point displacements of 1.0 mm or more from the image centre, were considered indicators of an unstable adjustment. During each iteration, new GCP sets were added where required, and individual GCPs with weak image correlation or poor adjustment statistics (i.e., if the displacement error of an individual GCP remained above 10.0 m after several iterations) were removed.

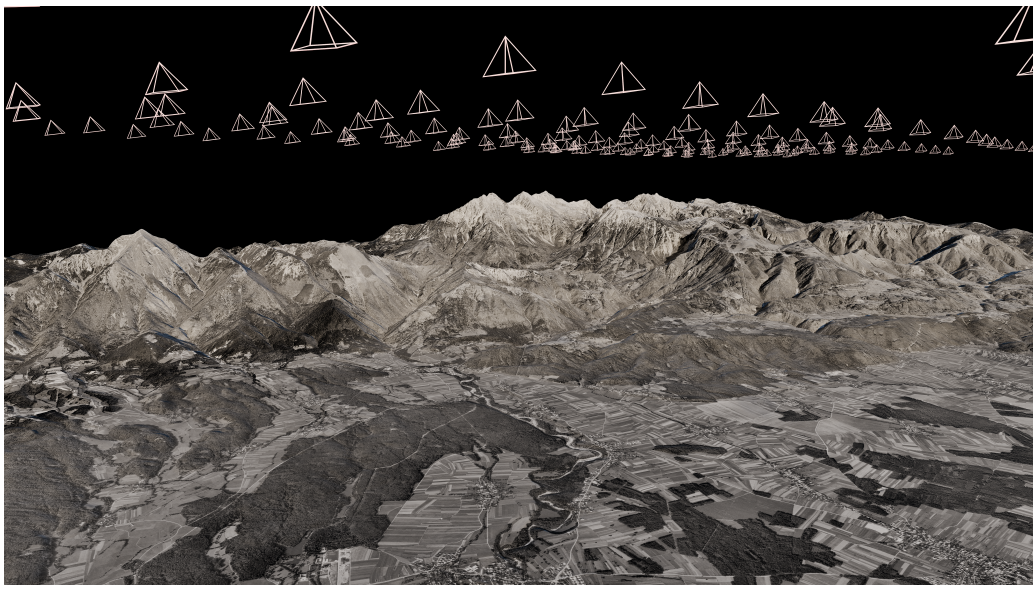


Figure 7. Camera positions reconstructed using SfM over the rugged relief of Kamnik-Savinja Alps.

Several strategies were used to handle exceptions to the regular processing procedure. If iterations diverged rather than converged, additional GCPs were introduced and the SfM bundle adjustment was rerun for the complete image set to obtain a substantially different parameter fit. In cases of substantial divergence of the estimated interior orientation parameters, the focal length was deliberately fixed to the value specified in the calibration report before rerunning the adjustment. If individual images failed to align, an additional step was used to align these exceptions to the existing tie point cloud; additional GCPs were added as needed. If an isolated image set had no overlap with already aligned material and could not be matched to the reference data, it was processed separately as an independent SfM workflow without a reference data. This approach was used for several isolated sets of 2–60 images from PAS1 acquisitions.

The 1953–1969 PAS1 acquisitions were particularly heterogeneous. They included a substantial proportion of contact print images, many calibration groups, and several linear acquisitions with only one dimensional overlap. As a result, the complete block adjustment could not always converge to the required accuracy. After an initial bundle adjustment,

such projects were split into yearly or smaller subprojects, and optimization was performed separately for each subproject.

The output of bundle adjustment was a fully optimized set of exterior orientation parameters for all cameras and optimized interior orientation parameters for all camera calibration groups.

4.4. Orthomosaic Generation and Production of Results

Orthorectification was performed using the DTM 12.5 m DEM (see Section 3.5). During orthorectification, images were projected onto the DEM using the optimized exterior orientation parameters. Mosaicking was performed with the Metashape "Refine seamlines" parameter, which helps avoid seamlines crossing high buildings. Before orthomosaic export, larger cloud formations were manually masked. The orthomosaics were generated in the Slovenian national projection (EPSG 3794), at a uniform spatial resolution of 0.5 m, even though some PAS1 acquisitions would support higher resolution.

5. Results

Of the 85,969 HAPs considered, 83,467 images (97.1%) were successfully processed. 2436 images (2.8%) were excluded from processing because they consisted of Luftwaffe images, infrared imagery, panoramic imagery, or other material outside the project scope. Only 66 images (0.08%) failed to complete the AT step successfully.

The main processing outputs are 45 annual orthomosaic products for the period between 1953 and 2005. Contrary to conventional photogrammetric practice, the orthomosaics were generated using the entire extent of each source aerial photograph, including the areas up to the physical image edges. This approach was adopted to preserve as much of the original visual information as possible. One orthomosaic was produced for each year with acquisitions in this interval, therefore no orthomosaics were produced for years 1955, 1958, 1965, 1978–1979, and 1982–1984. Figure 8 shows a short time series of a small area in Slovenia. In this example, the potential to detect changes from the orthomosaics is clearly evident. Aerial triangulation accuracies are summarized in Table 4, while final orthomosaic accuracies are discussed in Section 5.1.

The accuracy of the aerial triangulation was computed using ICPs that were manually selected in each processing block. Each block from 1970 onwards had approximately 40 ICPs. In the years before 1970, the processing was carried out in smaller patches that had at least 100 HAPs. The RMSE values in Table 4 present the average of these smaller blocks for each year. The RMSE of AT was assessed per block of years for years from 1970 onwards, and per partes on individual blocks for years up to 1970. For the latter, the displayed values are for blocks containing at least 100 HAPs (except for 1953, which contains only 32). The results show a clear trend, with lower accuracies in the earliest years and higher accuracies in the most recent years. From 1988 the RMSE is always below 2 m, which is approximately twice as good as in the earliest years. Although the oldest block had more GCPs, this trend was expected, as older HAPs can be more deformed and generally in worse condition. The processing of smaller blocks with smaller image overlap also leads to lower accuracies.

The produced orthomosaics were tiled into 1 × 1 km tiles. Because the number of HAPs varies strongly by year, from 11 to 5013 images, the number of tiles also varies, from 108 to 23,306 tiles per year. The annual coverage of Slovenia ranges from 0.4% to 98.8% (for detailed annual data on coverages see Table 6 in Section 5.2). Approximate average national coverage is 12% for early PAS1 years (1953–1969), 28% for late PAS1 years (1970–1974), and 40% for analogue CAS acquisitions (1975–2005). Frequencies of PAS1 and CAS annual orthomosaics are shown on Figure 9. In 19 PAS1 years the major cities were acquired 10–12 times, and main transportation corridors at least 5 times. On the other hand, more

than 50% of the country was acquired only 1 or 2 times. In 26 CAS yearly campaigns the majority of Slovenia was acquired at least 9 times, with the exception of the military zone Gotenica (south-eastern Slovenia, close to the border with Croatia), which was not acquired before 1990. More frequent acquisitions, up to 19, occurred in the overlapping edges of CAS yearly blocks.

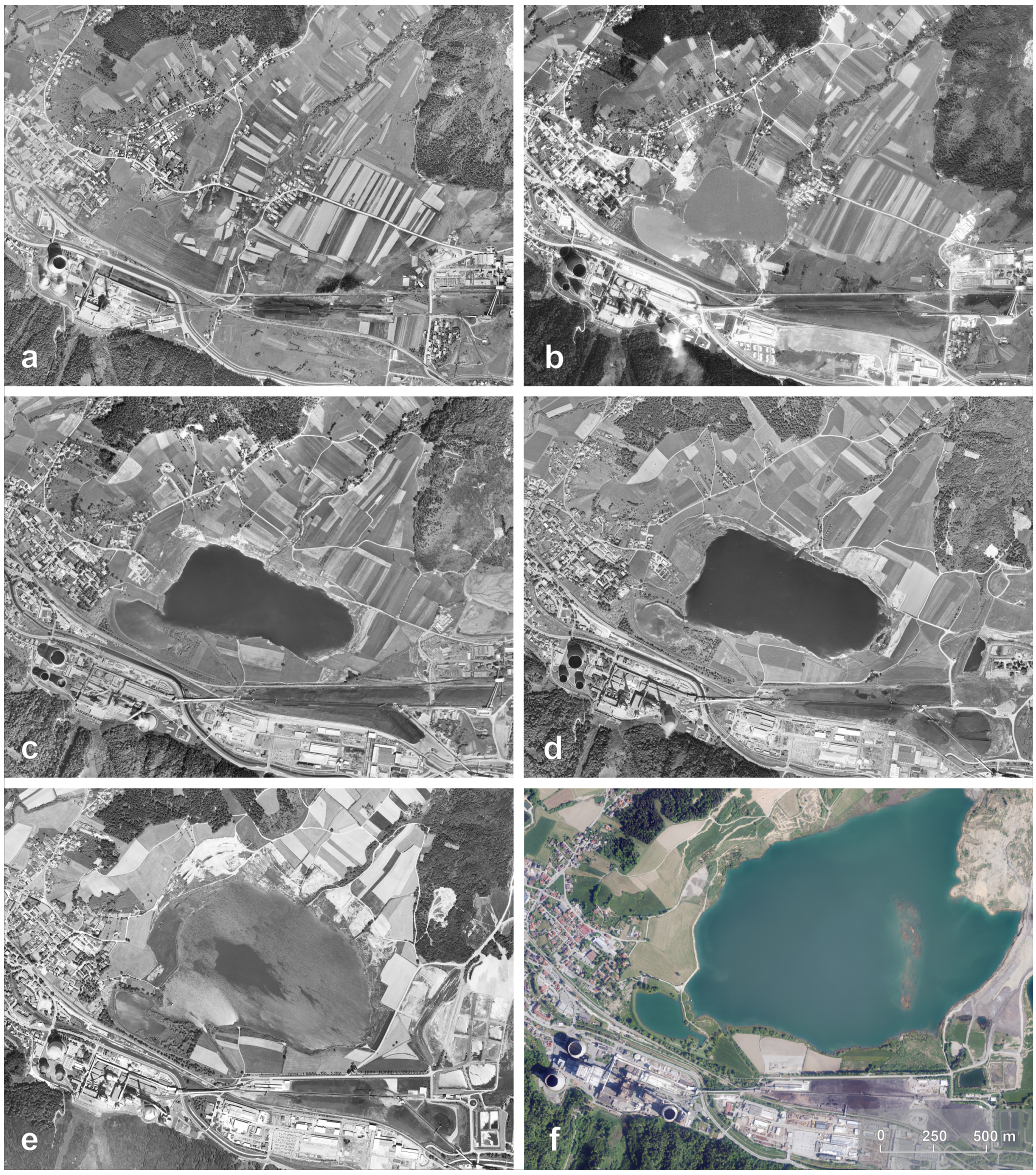


Figure 8. Crop from the produced orthoimages from the following archive years 1973 (**a**), 1980 (**b**), 1987 (**c**), 1993 (**d**) and 2005 (**e**), as well as the current orthophoto image from 2025 (**f**). Severe degradations due to the underground Velenje Coal Mine are clearly visible. In a timespan of several decades, the land slowly subsided, the village of Družmirje submerged (and had to be abandoned), and a new artificial lake that was formed on the subsided area grew steadily.

Each orthomosaic is accompanied with corresponding supplementary products, which were prepared during the final processing phase. These are: a small preview image, vector layer containing footprints (extents of aerial images on the ground), vector layer containing seamlines, textual CSV file containing six exterior orientation parameters of all cameras at the moment of acquisition (i.e., X, Y, Z; ϕ, ω, κ), and Excel file containing metadata from all produced tiles (production information; accuracy along with a list of all source HAPs that contribute pixels to the individual tile).

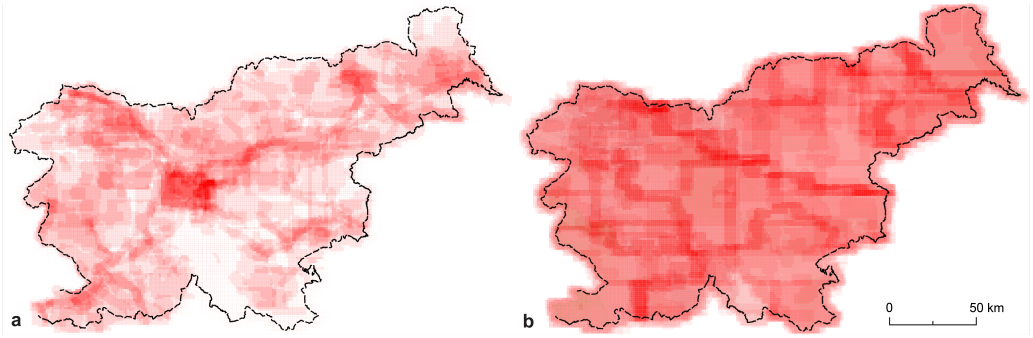


Figure 9. Frequency of (**a**) PAS1 and (**b**) CAS annual coverages. While the PAS1 orthomosaics are primarily oriented towards major cities and main transportation corridors, the CAS orthomosaics cover the whole country quite uniformly.

5.1. Accuracy Assessment of the Orthomosaics

The planimetric accuracy of the orthomosaics was evaluated using CHKs, while the mismatch along the seamlines was assessed visually.

Planimetric accuracy was evaluated using the Root Mean Square Error (RMSE). A total of 120 CHKs were evenly distributed across Slovenia (Figure 10a). These CHKs were digitized from recent 25 cm CAS national orthophotos acquired in 2021–2023. For PAS1 years, additional CHKs had to be selected because the corresponding orthomosaics cover only limited areas or narrow strips (e.g., Figure 2a,b), leaving many of the 120 standard CHKs outside the archive coverage (Figure 10b).

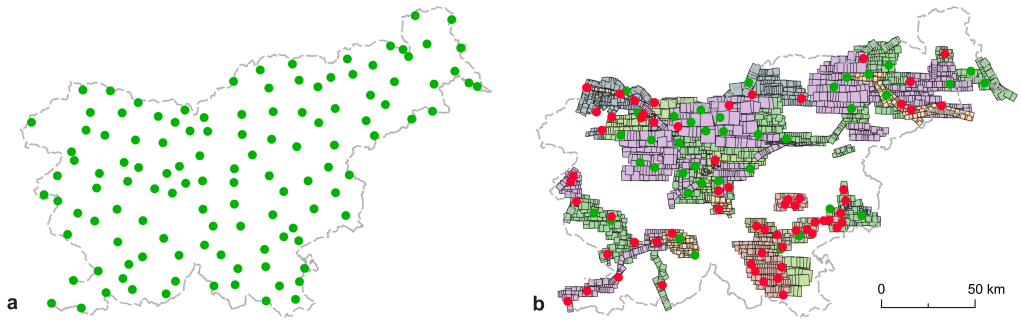


Figure 10. (**a**) Distribution of 120 normally used CHKs over Slovenia. (**b**) Distribution of CHKs for PAS block 1961–1969; background are footprints of HAPs of those years; standard CHKs are depicted in green, CHKs newly selected for this block in red.

Accuracy assessment was performed on a yearly basis, but not necessarily for each year individually. Instead, accuracy was evaluated for groups of years processed together in the same Metashape project.

Table 5 and Figure 11a indicate a general improvement in orthomosaic positional accuracy over time, reflected in the overall decrease in RMSE. The oldest orthomosaics, covering the 1953–1960 period, have a combined planimetric RMSE of 3.26 m, whereas the most recent period, 2001–2005, has an RMSE of only 1.46 m. To further assess the distribution of positional errors over the entire period under consideration, the 95th percentile and median of the combined planimetric deviations were calculated. The 95th percentile is 4.15 m, meaning that 95% of the check points have a combined planimetric positional deviation of 4.15 m or less. The median is 1.32 m. The difference between the median and RMSE indicates that the RMSE is influenced by a relatively small number of larger, but valid, positional deviations. Those are mostly located in alpine regions with elevations above 1200 m (Figure 11b).

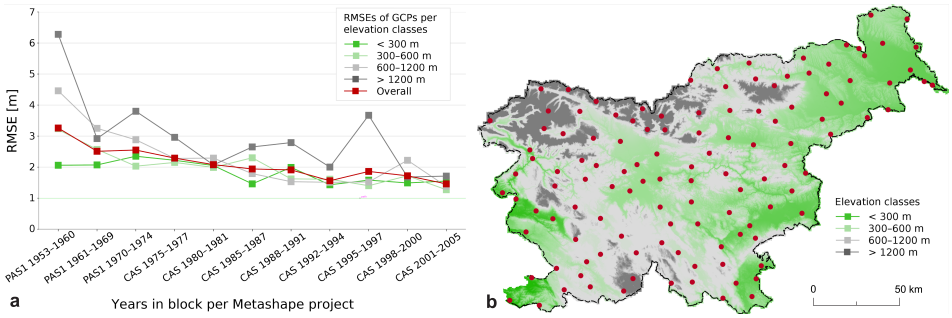


Figure 11. The diagram (**a**) illustrates an improving trend in orthomosaic positional accuracy (RMSE) over time. When Slovenia is divided into four elevation classes (**b**) using thresholds of 300 m, 600 m, 1200 m and above 1200 m, the classes contain 50, 38, 20 and 12 GCPs, respectively. The GCPs in the fourth elevation class, concentrated in the Alpine regions of north-western and northern Slovenia, have the largest RMSE errors in most blocks (**a**).

The ASPRS standard, in addition to positional accuracy, provides guidelines for seamline mismatch in orthophotos. Seamline deviations should not exceed twice the RMSE value [39]. These deviations were not checked systematically, but only visually around several random point locations. At these locations, the inspected seamlines do not exceed the ASPRS threshold. Some identified small mismatches are mainly observed on the road network (e.g., Figure 12b).

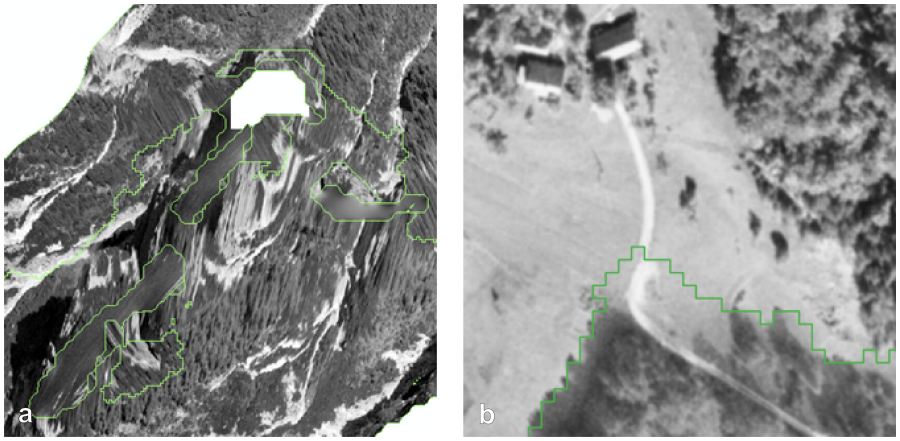


Figure 12. (**a**) Example of artifacts and small gaps in mountainous area in Kamnik and Savinja Alps from 1992. (**b**) Visible split in a local road along the seamline caused by imperfect alignment in hilly terrain in central Slovenia on the 1999 orthomosaic.

During the visual inspection of orthomosaics and seamlines, several areas with gaps or artifacts were identified in the final mosaic. These occur mainly at the edges of aerial survey blocks, in mountainous regions, and in areas with complex terrain (Figure 12a). The artefacts are primarily the result of the decision that no edge buffer or no-overlap-based trimming was applied, so also peripheral areas with weak overlap, as well as areas with no overlap with neighbouring photographs, were retained.

5.2. Accuracy of the Initial Camera Positions

In order to assess the accuracy of the initial camera positions provided in the metadata, we compared them with the image positions estimated through aerial triangulation (Table 6). The results reveal substantial year-to-year variation in the accuracy of the initial camera positions. As expected, the most recent CAS acquisitions (2000–2005) generally exhibit the highest positional accuracy, with median errors decreasing from 19.4 m in 2000 to 9.4 m in

2005. In contrast, many of the older acquisitions show median positional errors of several hundred meters, while individual images may be displaced by several kilometers.

The large differences between the mean, median, and RMSE values for several acquisition years further indicate that the error distributions are strongly affected by a limited number of extreme positional errors (Figure 13: example for the year 1975). Across the complete dataset, the mean positional error is 652.4 m and the median is 315.5 m, whereas the RMSE reaches 2157.3 m. Particularly pronounced discrepancies occur in some acquisition years. For example, the 1980 imagery has a median error of 678.5 m but an RMSE of 11.3 km, while the 1999 imagery has a median error of only 47.5 m but an RMSE of 1.54 km. These differences show that the initial metadata for most HAPs in these acquisitions was relatively accurate, while a smaller number of HAPs contain very large positional errors. These discrepancies may be attributed to errors in the initial camera positions, which were manually estimated from existing topographic maps before the advent of computer-assisted georeferencing and were therefore susceptible to interpretation and transcription errors (see also Section 3.3).

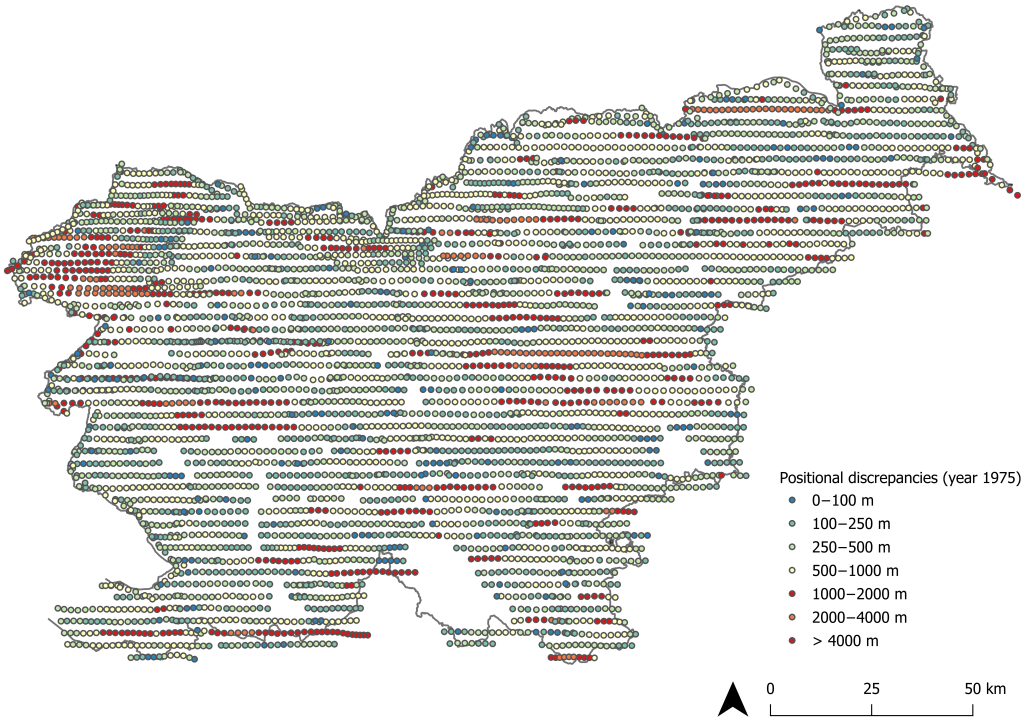


Figure 13. Planimetric discrepancies between the initial camera positions provided in the metadata and the image positions estimated through aerial triangulation for images acquired in 1975.

5.3. Accuracy of Calculated Camera Geometries

For survey years with available camera calibration reports, the reported calibration parameters were compared with those estimated during SfM processing in Agisoft Metashape. Where multiple camera calibration groups were available for a given year, results from selected representative groups are presented in Table 7. The closest agreement between the reported and estimated parameters was generally observed for larger calibration groups containing HAPs digitised from original film negatives. In contrast, groups containing fewer HAPs (e.g., calibration report dated 1976-02-16) or images digitised from contact prints (e.g., report dated 1970-01-14) exhibited somewhat larger discrepancies. In these cases, the absolute differences between the estimated principal point coordinates (c_x, c_y) and their corresponding values in the historical calibration reports exceeded 0.2 mm. Never-

theless, the overall agreement between the historical and estimated calibration parameters remained satisfactory.

Table 7. Comparison of camera geometry parameters obtained from calibration reports and those calculated in the model. Comparisons are shown only for cases where the year of acquisition is the same as the year of the report (in exceptional cases in the previous or the following year), and for a few representative camera calibration groups only (if more than one exists). Explanation of some entries: the key relating this table to Table 2 is the date code in the column "Date of report". The column "Calib(ration) gr(oup)" contains, in addition to the group ID, information on which type of images are in the group: either scanned negative films ("neg. f.") or scanned contact prints ("cont. pr."). Values "n.a." in columns "cx" and "cy" denote cases where the values of the principal point could not be inferred from the calibration report. Values "Fixed" in the column "F(ocal) l(ength)" indicate that the focal length had to be set as fixed in the model; otherwise divergence occurred in the AT process.

Date of Report	Calibration Report Data			Metashape Model Data per Calibration Group				
	F. l. [mm]	cx	cy	Calibr. gr.	n. HAPs	F. l. [mm]	cx	cy
14-01-1970	152.700	−0.001	−0.004	neg. f. 152	1361	Fixed	0.048	0.014
14-01-1970	152.700	−0.001	−0.004	cont. p. 152	60	Fixed	0.376	0.307
28-04-1975	152.980	n.a.	n.a.	neg. f. 27	212	153.146	−0.031	−0.072
28-04-1975	152.980	n.a.	n.a.	cont. p. 31	246	Fixed	−0.022	0.082
28-04-1975	152.980	n.a.	n.a.	neg. f. 33	171	Fixed	0.138	0.077
28-04-1975	152.980	n.a.	n.a.	cont. p. 35	244	Fixed	0.003	−0.082
16-02-1976	152.690	0.002	0.012	neg. f. 29	6	152.190	−0.287	0.119
10-04-1984	305.330	0.000	−0.010	neg. f. 305	2116	304.780	0.084	−0.066
02-03-1987	210.750	0.010	0.010	neg. f. 210	1553	210.524	0.106	0.039
23-09-1992	210.750	0.010	0.010	neg. f. 26	230	210.778	0.0243	−0.022
23-09-1992	210.750	0.010	0.010	neg. f. 32	210	210.761	−0.009	0.109
23-09-1992	210.750	0.010	0.010	neg. f. 34	226	210.966	0.007	0.115
16-02-1996	305.328	0.011	0.002	neg. f. 305	652	305.061	0.071	−0.042
21-02-1996	210.745	0.007	0.002	neg. f. 210	837	210.937	0.066	0.058
21-02-1996	210.745	0.007	0.002	neg. f. 210	2070	210.710	0.037	−0.019
08-01-1999	153.593	0.001	−0.002	neg. f. 154	1164	153.507	0.049	−0.039
19-02-1999	210.749	0.006	0.003	neg. f. 25	268	211.054	0.003	−0.007
19-02-1999	210.749	0.006	0.003	neg. f. 27	113	211.412	0.101	0.007
19-02-1999	210.749	0.006	0.003	neg. f. 28	265	210.693	0.087	−0.032
19-02-1999	210.749	0.006	0.003	neg. f. 42	18	210.824	0.115	0.070
21-01-2002	153.600	0.003	−0.004	neg. f. 154	1494	153.548	0.041	−0.009
12-02-2004	153.600	0.002	−0.005	neg. f. 154	1039	153.628	0.040	−0.029

5.4. Breakdown of Manual Effort and Computation Times

Although the overall methodology remained consistent throughout the project, individual processing steps were continuously refined and adapted to address challenges encountered during implementation. These challenges became increasingly frequent and complex when processing older imagery, requiring adjustments to the preprocessing procedures and processing parameters. Consequently, not all image blocks were processed using identical procedures, limiting the possibility of direct quantitative comparisons of processing times and manual effort across different years.

AT was the most computationally demanding stage of the workflow. Processing was performed using Agisoft Metashape in a two-node network processing configuration comprising two Windows 10 workstations. The first was equipped with a 32-core AMD Ryzen Threadripper PRO 5975WX processor, 256 GB of DDR4 RAM, and two NVIDIA RTX A4500 GPUs. The second featured a 12-core Intel Xeon W-2265 processor, 256 GB of DDR4 RAM, and an NVIDIA Quadro RTX 5000 GPU. Computation times ranged from several hours to approximately two days per processing block, depending primarily on the number of HAPs within the block. Some blocks required repeated processing due to divergence during bundle adjustment, further increasing the overall computational effort.

Preprocessing requirements varied considerably between image collections. For the more recent Leica CAS imagery (2001–2005), the extraction of frame masks and fiducial mark coordinates was fully automated, requiring only a few hours per processed year. In contrast, the earliest PAS imagery (1959–1969) required extensive corrections to the archival metadata, followed by a combination of automated and manual processing steps. These procedures required approximately five person-days per processed year. The automated preparation of final outputs and subsequent visual quality checks required an additional person-day per processed year.

Several tasks were performed only once during the project. The manual identification and measurement of GCPs, independent ICPs, and CHKs required at least 20 person-days, while the preparation and validation of the reference CAS 2006 layer required approximately 15 person-days.

6. Discussion

The significance of the presented workflow is twofold. First, it provides a systematic framework for preparing and homogenising a heterogeneous national archive of HAPs spanning more than five decades. The archive contains HAPs acquired using different cameras and film types and preserved and digitized under variable conditions. In addition, some acquisitions lack complete camera, flight, or calibration metadata, partly as a consequence of the historical development and transfer of the archive, including incomplete delivery of documentation from VGI Belgrade following the breakup of former Yugoslavia. Consequently, preprocessing could not be treated as a uniform batch operation. Visual inspection, radiometric correction, fiducial mark extraction, frame masking, metadata verification, and the treatment of individual image anomalies required a substantial amount of manual and semi automatic intervention. This illustrates an important characteristic of large historical aerial archives: the principal obstacle to archive scale processing is not necessarily photogrammetric reconstruction itself, but the preparation, standardisation, and quality control required before reliable image orientation can be performed.

Second, the results demonstrate that a very large number of HAPs can nevertheless be georeferenced within a constrained production period by combining several complementary strategies. These included SfM based AT, the systematic grouping of HAPs into calibration groups according to acquisition year, camera type, focal length, and scan type, and the use of existing reference data to support initial image matching and absolute positioning. The effectiveness of the workflow therefore results not from any single processing component, but from their integration. Calibration grouping reduced the heterogeneity introduced by different camera and digitization configurations, while the reference imagery provided a consistent spatial framework for the initial orientation of otherwise weakly georeferenced HAPs. Together, these measures enabled stable processing across imagery of substantially different ages and technical characteristics.

The positional accuracy of the resulting orthomosaics (see Table 5 and Figure 11) nevertheless varies between acquisition periods and geographical settings. Older orthomosaics generally exhibit slightly higher mean CHK RMSE values than more recent datasets. This trend should not, however, be interpreted as a direct consequence of image age alone. Older acquisitions are also more likely to be affected by deformation or degradation of film and contact prints, incomplete calibration information, differences in scanning quality, older camera systems, and less favourable or less well documented acquisition geometry. The comparatively small change in mean RMSE across the full temporal extent of the archive is therefore noteworthy and suggests that the workflow compensated effectively for much of this heterogeneity.

Mean RMSE alone does not fully characterize the spatial distribution of positional errors. The differences between median and 95th-percentile CHK errors indicate that error distributions are frequently skewed, with a relatively small number of locations exhibiting substantially larger residuals. These higher errors occur particularly in mountainous terrain (Figure 11). Several factors probably contribute to this pattern, including stronger relief, the number and spatial distribution of GCPs relative to CHKs, differences in image overlap, and weaker block geometry near the margins of individual acquisition areas. The influence of these factors is likely cumulative rather than attributable to a single source.

An important distinction should also be made between the internal geometric consistency of an orthophoto mosaic and its absolute positional accuracy. The production workflow prioritized coherent HAP blocks and smooth transitions between neighbouring HAPs in order to obtain seamless national mosaics. Absolute positioning was therefore not optimized through the introduction of the maximum possible number of GCPs. Where higher absolute positional accuracy is required, the workflow could be further constrained using a greater number of accurately measured and spatially well-distributed GCPs. The observed accuracy should therefore be understood partly as a consequence of the production strategy rather than as an upper limit of what could be obtained from the source HAPs.

A further issue concerns the temporal separation between the HAPs and the reference datasets used for AT. To reduce this temporal difference, the CAS 2006 AT results were used as the principal reference for HAPs acquired after 1991, whereas the CAS 1992–1994 AT results were used for earlier acquisitions (see Figure 4). For HAPs acquired before 1975, the CAS 1975–1977 AT results were also tested as an alternative reference. However, its use did not improve the results relative to the 1992–1994 reference dataset. The maximum temporal separation between the processed HAPs and the reference layer was therefore approximately four decades. Despite this substantial interval, the workflow remained sufficiently robust to orient the HAP blocks successfully.

This result is important because temporal differences between HAPs and contemporary reference datasets are a recognized difficulty in image matching. Changes in vegetation, agricultural patterns, infrastructure, settlement, and land use progressively reduce the number of features that remain visually stable between epochs. The successful processing of HAPs separated from the reference data by several decades therefore indicates that sufficient persistent spatial information remained available for matching at the scale required by the workflow. Nevertheless, this should not be interpreted as evidence that the temporal difference is irrelevant. Areas affected by major urban development, infrastructure construction, forest change, or other substantial landscape transformations are expected to provide fewer reliable correspondences and may consequently require additional control or manual intervention.

Temporal mismatch also exists between the HAPs and the 12.5 m DEM from 2005 used for orthorectification (see Section 3.5). For the oldest HAPs, this difference reaches approximately 52 years. In general, terrain elevation is more temporally stable than land cover or image texture, which makes the use of a temporally younger DEM less problematic than the equivalent use of a younger orthophoto. Nevertheless, localized topographic changes caused by quarrying, road construction, river engineering, landslides, excavation, embankment construction, or other natural and anthropogenic processes can introduce local discrepancies. The absence of widespread problems attributable to DEM age therefore indicates that the 2005 DEM was adequate for the intended national-scale products, rather than demonstrating that terrain remained unchanged over the entire period.

The workflow is best characterized as semi automated or human-in-the-loop rather than fully automated. Some operations could be executed automatically and consistently over large HAP sets, whereas other tasks required expert inspection or manual correction

because of the heterogeneity of the archive. This balance was important for maintaining product quality. Further automation is nevertheless possible, particularly for repetitive preprocessing and quality control tasks. For example, frame mask generation could be integrated directly with fiducial mark detection. Once fiducial marks establish the internal image coordinate system, their positions could also provide geometric constraints for automatically defining the usable image frame. Other promising developments include automated detection of anomalous calibration solutions, identification of poorly oriented images, consistency checks of archive metadata, and automatic proposal or extraction of control points from reference data.

Digitization itself remains another important bottleneck. Scanning tens of thousands of analogue photographs is time consuming even before photogrammetric processing begins, and automation at this stage could therefore substantially reduce the resources required for future archive scale projects. Robot assisted scanning pipelines already represent a promising development in this direction [40]. Combined with increasingly automated image preprocessing, orientation, reference data matching, and quality control, such systems could ultimately shift HAP archive processing from a predominantly project based activity toward a reproducible production workflow.

In essence, the principal contribution of the presented approach is not the elimination of manual intervention, nor the achievement of the maximum theoretically obtainable accuracy for individual photographs. Rather, it demonstrates that a heterogeneous national archive containing more than five decades of HAPs can be transformed into spatially consistent orthophoto products at scale by combining automation with targeted expert intervention. The results suggest that the most effective strategy for such archives is therefore neither a completely manual nor a fully automatic workflow, but a carefully designed sequence in which automation is applied to reproducible operations and human quality control is concentrated on the comparatively small number of cases where archival heterogeneity prevents reliable automatic processing.

Future Work

The products generated in this study should be regarded as a foundation for further exploitation of the archive rather than as its final processing stage. One immediate possibility is the production of substantially higher resolution orthophotos for selected acquisitions. Approximately 7% of the processed HAPs were acquired from flight heights below 1.2 km, with some acquisitions flown as low as approximately 350 m above ground. For such imagery, orthophotos with ground resolutions of approximately 10 cm, and in favourable cases potentially 5 cm, could be produced. These products could provide exceptionally detailed documentation of settlements, infrastructure, vegetation, archaeological features, and other elements of the recent historical landscape.

A second major extension concerns the PAS2 collection, which was not processed within the project. PAS2 covers approximately the same period as the analogue CAS collection, from 1975 to 2005, and therefore appears partly redundant at the temporal level. However, many PAS2 acquisitions were designed for specific local purposes and were flown at substantially lower altitudes than the systematic CAS surveys. They consequently contain considerably greater spatial detail in many areas. Processing the more than 50,000 images in this collection would therefore complement the existing national time series with very high-resolution coverage of selected locations and periods.

The HAPs acquired over Slovenia by the German Luftwaffe in 1943 represent another important extension of the temporal range of the archive. Because these photographs differ substantially from the PAS and CAS material in terms of acquisition characteristics, metadata, image organization, and reference information, they are unlikely to be processed efficiently

using the workflow described here without substantial modification. Their georeferencing should therefore be considered a separate processing task. Successful integration of this collection would, however, extend systematic aerial documentation of parts of Slovenia into the Second World War period and considerably increase the value of the archive for historical and landscape research.

The oriented HAP blocks also provide opportunities that extend beyond two-dimensional orthophoto production. Where sufficient stereo overlap, suitable image geometry, and adequate image quality are available, SfM-based reconstruction can be used to derive historical digital surface models. Such models would introduce a third spatial dimension into the temporal archive and enable quantitative investigation of changes in terrain and surface structure. Potential applications include the analysis of landslides and other geomorphological processes, changes in forest extent and structure, urban expansion, infrastructure development, quarrying and other anthropogenic terrain modification, as well as three-dimensional reconstruction and visualization of historical landscapes.

Additional information can also be extracted directly from the orthomosaic time series. Automated or semi automated analyses could include historical land cover classification, mapping of forest and built up areas, reconstruction of road and transportation networks, detection of settlement expansion, and identification of other long term landscape changes. The systematic spatial and temporal organization of the resulting archive makes it particularly suitable for such analyses because changes can be investigated over large areas using geometrically comparable datasets rather than individual unrectified HAPs.

7. Conclusions

Producing historical orthomosaics from HAPs at a national scale is a demanding task because of the heterogeneity of the source material, incomplete metadata, differences in camera systems and acquisition geometry, variable preservation and scanning quality, and the large volume of imagery involved. This study demonstrates that these challenges can nevertheless be addressed through a carefully designed workflow combining manual, semi automatic, and automated procedures. Using this approach, 83,467 HAPs from the PAS1 and CAS collections of the Slovenian national aerial archive were successfully georeferenced, covering the period from 1953 to 2005.

The processing resulted in 45 annual orthomosaics with a spatial resolution of 0.5 m, distributed in a 1 × 1 km tile grid, with overall accuracy (mean CHK RMSE values) ranging from 1.46 to 3.26 m. The orthomosaics are accompanied by vector layers containing image footprints and seamlines, as well as metadata describing image orientation and individual tiles. Because there was no systematic acquisition of photographs during the first decades, national coverage varies substantially among the annual products (see Table 6 and Figure 11). Despite large variations in image age, camera type, focal length, scan type, preservation condition, and availability of original metadata, the workflow produced spatially consistent products that satisfied the accuracy requirements defined for the project. An important outcome of the study is therefore not only the resulting orthophoto archive itself, but also the demonstration that heterogeneous collections of HAPs can be processed systematically at national scale within a production oriented workflow.

The resulting dataset provides repeated high resolution observations of the Slovenian landscape over more than five decades and substantially improves the accessibility and practical usability of the national historical aerial archive. Comparable systematic national scale processing of HAPs remains relatively uncommon. Perhaps the most notable example is the historical orthophoto programme of the Swiss Federal Office of Topography, swisstopo, which has processed more than 100,000 HAPs as part of its long-term aerial image programme [41]. The Slovenian dataset therefore represents an important contribution to

the growing number of initiatives aimed at transforming national analogue aerial archives from collections of individual photographs into directly usable geospatial time series.

To facilitate their use beyond the original project, the annual orthomosaics and corresponding seamline layers have been published through the GURS spatial data infrastructure and are available through a Web Map Service (WMS) on the e-Prostor portal (https://ipi.eprostor.gov.si/jv/ accessed on 9 September 2026). The service can be used free of charge. Providing the results through an established national spatial data platform is particularly important because it allows HAPs to be used together with contemporary geospatial datasets without requiring users to perform additional photogrammetric processing.

The principal achievement of this work is the transformation of a large and heterogeneous analogue aerial archive into a spatially consistent and readily accessible national geospatial dataset. The project demonstrates that archive scale processing does not require every stage to be fully automated. Instead, an effective strategy combines automation for repetitive and reproducible operations with targeted expert intervention where the variability of historical material prevents reliable automatic processing. The resulting orthomosaics have immediate value for public administration, research, education, heritage management, and general historical enquiry, while at the same time providing a basis for future high resolution orthophoto production, historical landscape reconstruction, automated landscape analysis, and the processing of additional archival collections. In this sense, the project not only recovers HAPs as images, but converts them into a long-term spatial record of landscape change that can be systematically analysed alongside contemporary geospatial data.

Author Contributions: Conceptualization, A.M. and L.Š.; methodology, L.Š., A.M. and Ž.K.; software, L.Š., P.Č. and P.P.; validation, P.P., V.B. and N.B.; formal analysis, L.Š. and P.P.; investigation, L.Š.; resources, A.M. and Ž.K.; data curation, P.P.; writing—original draft preparation, L.Š., A.M., V.B. and P.P.; writing—review and editing, Ž.K. and N.B.; visualization, P.P. and Ž.K.; supervision, A.M.; project administration, A.M. and B.P. All authors have read and agreed to the published version of the manuscript.

Funding: This research was funded by the Surveying and Mapping Authority of the Republic of Slovenia (GURS) under the project Georeferencing of archive aerial images (GAAF, C2562-24-000014), which was part of Slovenia's Recovery and Resilience Plan (NOO) and funded under the EU Recovery and Resilience Facility, and by the Slovenian Research and Innovation Agency (ARIS) under the projects P6-0079, J2-4488, J7-70247, and GC-0006.

Institutional Review Board Statement: Not applicable.

Informed Consent Statement: Not applicable.

Data Availability Statement: Source data is unavailable due to privacy. Results are publicly available at link https://ipi.eprostor.gov.si/jv/ accessed on 9 September 2026; under the drop down menu set layer "Archive orthophotos" (only in Slovene language).

Conflicts of Interest: Co-author B.P. is an employee of the GURS, which funded this research project. The remaining authors declare that they have no known competing financial interests or personal relationships that could have appeared to influence the work reported in this paper.

Abbreviations

The following abbreviations are used in this manuscript:

AT	aerial triangulation
CAS	Cyclic Aerial Survey of Slovenia (analogue: 1975–2005; digital: from 2006 onward)
CHK	check point (used to assess orthomosaic accuracy)
CLAHE	Contrast Limited Adaptive Histogram Equalization
CSV	comma-separated values

DEM	digital elevation model
DLT	Direct Linear Transform
DPI	dots per inch
DSM	digital surface model
DTM	digital terrain model
GCP	ground control point
GNSS	Global Navigation Satellite System
GPS	Global Positioning System
GURS	Surveying and Mapping Authority of the Republic of Slovenia
GZS	Geodetic office of Slovenia
HAP	historical aerial photograph
hDSM	historical digital surface models
ICP	independent check point (used to assess model accuracy)
INS	Inertial Navigation System
RMSE	Root Mean Square Error
RS	recording sheet
PAS	Special Aerial Survey of Slovenia (PAS1: 1953–1974; PAS2: 1975–2005)
SfM	Structure from Motion
VGI	Military Geographical Institute, Belgrade, Serbia
WMS	Web Map Service

References

1. Morgan, J.L.; Gergel, S.E. Quantifying historic landscape heterogeneity from aerial photographs using object-based analysis. *Landsc. Ecol.* **2010**, *25*, 985–998. [CrossRef]
2. Kostrzewa, A. Geoprocessing of archival aerial photos and their scientific applications: A review. *Rep. Geod. Geoinform.* **2024**, *118*, 1–16. [CrossRef]
3. Cowley, D.C.; Stichelbaut, B.B. Historic aerial photographic archives for European archaeology. *Eur. J. Archaeol.* **2012**, *15*, 217–236. [CrossRef]
4. Sevara, C.; Verhoeven, G.; Doneus, M.; Draganits, E. Surfaces from the Visual Past: Recovering High-Resolution Terrain Data from Historic Aerial Imagery for Multitemporal Landscape Analysis. *J. Archaeol. Method Theory* **2018**, *25*, 611–642. [CrossRef] [PubMed]
5. Pinto, A.T.; Gonçalves, J.A.; Beja, P.; Pradinho Honrado, J. From archived historical aerial imagery to informative orthophotos: A framework for retrieving the past in long-term socioecological research. *Remote Sens.* **2019**, *11*, 1388. [CrossRef]
6. Hong, X.; Roosevelt, C.H. Orthorectification of large datasets of multi-scale archival aerial imagery: A case study from Türkiye. *J. Geovis. Spat. Anal.* **2023**, *7*, 23. [CrossRef]
7. Craciun, D.; Le Bris, A. Automatic algorithm for georeferencing historical-to-nowadays aerial images acquired in natural environments. *Int. Arch. Photogramm. Remote Sens. Spat. Inf. Sci.* **2022**, *XLIII-B2-2022*, 21–28. [CrossRef]
8. Kim, J.S. Near-automated orthorectification of archived aerial photographs. *J. Appl. Remote Sens.* **2022**, *16*, 036505. [CrossRef]
9. Knuth, F.; Shean, D.; Bhushan, S.; Schwat, E.; Alexandrov, O.; McNeil, C.; Dehecq, A.; Florentine, C.; O'Neel, S. Historical Structure from Motion (HSfM): Automated processing of historical aerial photographs for long-term topographic change analysis. *Remote Sens. Environ.* **2023**, *285*, 113379. [CrossRef]
10. Gonçalves, J.A. Automatic orientation and mosaicking of archived aerial photography using Structure from Motion. *Int. Arch. Photogramm. Remote Sens. Spat. Inf. Sci.* **2016**, *XL-3/W4*, 123–126. [CrossRef]
11. Schönberger, J.L.; Frahm, J.-M. Structure-from-Motion Revisited. In Proceedings of the IEEE Conference on Computer Vision and Pattern Recognition (CVPR), Las Vegas, NV, USA, 27–30 June 2016; pp. 4104–4113.
12. Mölg, N.; Bolch, T. Structure-from-Motion using historical aerial images to analyse changes in glacier surface elevation. *Remote Sens.* **2017**, *9*, 1021. [CrossRef]
13. Suh, J.W.; Ouimet, W. Generation of high-resolution orthomosaics from historical aerial photographs using Structure-from-Motion and lidar data. *Photogramm. Eng. Remote Sens.* **2023**, *89*, 37–46. [CrossRef]
14. Karel, W.; Doneus, M.; Verhoeven, G.; Briese, C.; Ressl, C.; Pfeifer, N. OrientAL—Automatic Geo-Referencing and Ortho-Rectification of Archaeological Aerial Photographs. *ISPRS Ann. Photogramm. Remote Sens. Spat. Inf. Sci.* **2013**, *II-5/W1*, 175–180. [CrossRef]

15. Karel, W.; Doneus, M.; Briese, C.; Verhoeven, G.; Pfeifer, N. Investigation on the Automatic Geo-Referencing of Archaeological UAV Photographs by Correlation with Pre-Existing Ortho-Photos. *Int. Arch. Photogramm. Remote Sens. Spat. Inf. Sci.* **2014**, *XL-5*, 307–312. [CrossRef]
16. Rault, C.; Dewez, T.J.B.; Aunay, B. Structure-from-Motion Processing of Aerial Archive Photographs: Sensitivity Analyses Pave the Way for Quantifying Geomorphological Changes Since 1978 in La Réunion Island. *ISPRS Ann. Photogramm. Remote Sens. Spat. Inf. Sci.* **2020**, *V-2-2020*, 773–780. [CrossRef]
17. Maiwald, F.; Maas, H.-G. An Automatic Workflow for Orientation of Historical Images with Large Radiometric and Geometric Differences. *Photogramm. Rec.* **2021**, *36*, 77–103. [CrossRef]
18. Feurer, D.; Vinatier, F. Joining multi-epoch archival aerial images in a single SfM block allows 3-D change detection with almost exclusively image information. *ISPRS J. Photogramm. Remote Sens.* **2018**, *146*, 495–506. [CrossRef]
19. Child, S.F.; Stearns, L.A.; Girod, L.; Brecher, H.H. Structure-from-Motion photogrammetry of Antarctic historical aerial photographs in conjunction with ground control derived from satellite data. *Remote Sens.* **2021**, *13*, 21. [CrossRef]
20. Persia, M.; Barca, E.; Greco, R.; Marzulli, M.I.; Tartarino, P. Archival aerial images georeferencing: A geostatistically-based approach for improving orthophoto accuracy with minimal number of ground control points. *Remote Sens.* **2020**, *12*, 2232. [CrossRef]
21. Heisig, H.; Simmen, J.-L. Re-engineering the Past: Countrywide Geo-referencing of Archival Aerial Imagery. *PFG J. Photogramm. Remote Sens. Geoinf. Sci.* **2021**, *89*, 487–503. [CrossRef]
22. Mestre-Runge, C.; Lorenzo-Lacruz, J.; Ortega-Mclear, A.; Garcia, C. An Optimized Workflow for Digital Surface Model Series Generation Based on Historical Aerial Images: Testing and Quality Assessment in the Beach-Dune System of Sa Ràpita-Es Trenc (Mallorca, Spain). *Remote Sens.* **2023**, *15*, 2044. [CrossRef]
23. Institut National de L'information Géographique et Forestière (IGN). *BD ORTHO® Historique, Version 1.0–Descriptif de Contenu*; IGN: Paris , France, 2021. Available online: https://data.geopf.fr/annexes/ressources/documentation/DC_BDORTHOHisto_1-0.pdf (accessed on 9 September 2026).
24. Lantmäteriet. *Product Description: Historical Orthophotos (Historiska Ortofoton)*; Lantmäteriet: Gävle, Sweden, 2023. Available online: https://www.lantmateriet.se/globalassets/geodata/geodataprodukter/flyg--och-satellitbilder/e_hist_ortofoto.pdf (accessed on 9 September 2026).
25. National Land Survey of Finland. NLS Orthophotos. Available online: https://www.maanmittauslaitos.fi/en/maps-and-spatial-data/datasets-and-interfaces/product-descriptions/orthophotos (accessed on 9 September 2026).
26. Šafář, V.; Staňková, H.; Pospíšil, J.; Kaňa, D. Archive and wartime aerial photographs and procedures of their treatment. *Int. Arch. Photogramm. Remote Sens. Spat. Inf. Sci.* **2020**, *XLIII-B2-2020*, 69–74. [CrossRef]
27. Kardoš, M.; Tuček, J.; Slatkovská, Z.; Tomaštík, J. Historická ortofotomapa Slovenska—analýza polohovej presnosti a jej aplikácie pri identifikácii parciel. *Kartogr. Listy* **2017**, *25*, 37–47.
28. Hellenic Military Geographical Service. Aerial Photography. Available online: https://www.gys.gr/hmgs-aerial_en.html (accessed on 9 September 2026).
29. Pérez, J.A.; Bascón, F.M.; Charro, M.C. Photogrammetric usage of 1956–57 USAF aerial photography of Spain. *Photogramm. Rec.* **2014**, *29*, 108–124. [CrossRef]
30. Johansen, K.L.; Laursen, S.T. Gravhøje set fra luften: En kildekritisk undersøgelse. *Kuml* **2007**, *56*, 47–72. [CrossRef]
31. Perko, D.; Ciglič, R.; Zorn, M. (Eds.) *The Geography of Slovenia: Small But Diverse*, 1st ed.; Springer International Publishing: Cham, Switzerland, 2020. [CrossRef]
32. Digital Elevation Model (Surveying and Mapping Authority of the Republic of Slovenia). Available online: https://eprostor.gov.si/imps/srv/api/records/4ac9a90e-7694-42eb-870a-c11ef93783c4 (accessed on 9 September 2026).
33. Kostrzewa, A.; Farella, E.M.; Morelli, L.; Ostrowski, W.; Remondino, F.; Bakuła, K. Digitizing Historical Aerial Images: Evaluation of the Effects of Scanning Quality on Aerial Triangulation and Dense Image Matching. *Appl. Sci.* **2024**, *14*, 3635. [CrossRef]
34. Agisoft Metashape Professional User Manual, Version 2.1. Available online: https://www.agisoft.com/pdf/metashape-pro_2_1_en.pdf (accessed on 9 September 2026).
35. Agisoft Metashape Python Reference, Release 2.1.1. Available online: https://www.agisoft.com/pdf/metashape_python_api_2_1_1.pdf (accessed on 9 September 2026).
36. Falkner, E.; Morgan, D. *Aerial Mapping: Methods and Applications*, 2nd ed.; CRC Press: Boca Raton, FL, USA, 2002.
37. Schenk, T. *Introduction to Photogrammetry*; Department of Civil and Environmental Engineering and Geodetic Science, The Ohio State University: Columbus, OH, USA, 2005.
38. Brown, D.C. Decentering distortion of lenses. *Photogramm. Eng.* **1966**, *32*, 444–462.
39. American Society for Photogrammetry and Remote Sensing (ASPRS). *ASPRS Positional Accuracy Standards for Digital Geospatial Data*, 2nd ed.; Version 2; ASPRS: Baton Rouge, LA, USA, 2024.

40. Masson, S.; Potts, A.; Williams, A.; Berggreen, S.; McLaren, K.; Martin, S.; Noda, E.; Nordfors, N.; Ruecroft, N.; Druckenmiller, H.; et al. A robot-assisted pipeline to rapidly scan 1.7 million historical aerial photographs. *npj Herit. Sci.* **2026**, *14*, 123. [CrossRef]
41. Federal Office of Topography swisstopo. A Journey Through Time–Aerial Images. Available online: https://www.swisstopo.admin.ch/en/timetravel-aerial-images (accessed on 17 August 2026).

Disclaimer/Publisher's Note: The statements, opinions and data contained in all publications are solely those of the individual author(s) and contributor(s) and not of MDPI and/or the editor(s). MDPI and/or the editor(s) disclaim responsibility for any injury to people or property resulting from any ideas, methods, instructions or products referred to in the content.